Research Square

Preprints are preliminary reports that have not undergone peer review.
They should not be considered conclusive, used to inform clinical practice,
or referenced by the media as validated information.

Acoustic wave fluctuations in nonthermal solar plasma

Souvik Das
Tezpur University
Atteya Ahmed
Alexandria University
PK Karmakar
pkk@tezu.ernet.in

Tezpur University

Article

Keywords:

Posted Date: June 23rd, 2026

DOI: https://doi.org/10.21203/rs.3.rs-9947679/v1

License: This work is licensed under a Creative Commons Attribution 4.0 International License.
Read Full License

Additional Declarations: No competing interests reported.

Acoustic wave fluctuations in nonthermal solar plasmas

Souvik Das[1], **Ahmed Atteya**[2], **and Pralay Kumar Karmakar**[1,*]

[1]Department of Physics, Tezpur University, Napaam, Tezpur, Sonitpur, Assam - 784028, India
[2]Department of Physics, Faculty of Science, Alexandria University, Alexandria - 21511, Egypt
[*]pkk@tezu.ernet.in

ABSTRACT

It is well-known that solar plasmas exhibit a spectral plethora of collective oscillatory modes, alongside fluctuations, actively illuminating involved dynamical and helioseismic phenomena. In this study, a linear acoustic fluctuation analysis is performed to explore the stability of nonthermal κ-modified viscoturbulent inhomogeneous solar plasmas. The intrinsic fluid turbulence effects are properly incorporated using a modified Larson logabarotropic equation of state. The analysis yields a generalized linear cubic dispersion relation describing the self-gravitationally bounded solar interior plasma fluctuations. We explore the influence of key physical parameters—including the nonthermality index, electron temperature, dynamic viscosity, and thermal conductivity—on the fluctuation dispersion signatures. The Routh–Hurwitz stability criterion is systematically applied to assess the plasma stability features. Both the distinct classes of helioseismic modes, *g*-modes and *p*-modes, are methodically characterized. While, the *g*-modes can induce large changes to the solar parameters, they cease to exhibit oscillatory behaviours beyond approximately 2.4×10^8 m from the solar core. In contrast, the *p*-modes propagate throughout the Sun. The excitation of the ubiquitous five-minute oscillations is illustratively analysed and observationally validated. This investigation indicates that electron nonthermality spectral index κ and thermal conductivity enhance mode propagation, whereas the plasma viscosity and electron temperature act as damping factors. The radially outward energy flux of the photospheric *p*-modes is estimated to lie in the range of $10^5 - 10^6$ W m^{-2}. These *p*-modes are shown to contribute substantially to chromospheric spicule formation via the longitudinal-to-transverse mode conversion mechanism. The κ-modified fluctuations studied here fairly align with the prior solar observational predictions.

1 Introduction

The morphodynamics and evolution of the solar interior remain among the most enduring and incompletely understood challenges in solar physics. Distinct types of waves and oscillation modes pervade the solar plasma across all spatiotemporal scales[1–4]. These waves serve as powerful diagnostic tools, offering critical insights into the dynamic and structural properties of the solar interior[3,5–9]. In this context, probing the Sun and its interior in light of the collective helioseismic waves has been one of the engaging topics among the solar researchers for decades. These collective non-radial modes are produced in the form of standing acoustic waves excited stochastically by turbulence at the convective zone[10,11]. Subsequently, these modes get trapped within the solar interior and are sustained by the restoring forces of solar thermal (acoustic) pressure.

Depending on the driving physical mechanisms, helioseismic waves are broadly classified into two categories: (i) Thermal pressure-driven acoustic waves (pressure modes or *p*-modes) and (ii) Buoyancy-driven internal gravity waves (gravity modes or *g*-modes)[12–16]. The *p*-modes are high-frequency waves that propagate throughout much of the solar interior, reflecting off deeper layers before returning to the surface, thereby conveying diagnostic information about subsurface solar structure[5,12,14]. Precise spectroscopic Doppler shift observations have already detected the five-minute oscillation of solar surface[5,12,17].

Helioseismology, through detailed analysis of *p*-modes, has significantly advanced our understanding of the solar interior structure, as depicted in the standard solar models (SSMs)[1,3,7]. Besides, the *g*-modes—characterized by their long wavelengths and low frequencies—get trapped beneath the radiative zone and hence remain extremely challenging to detect at the surface[13,17,18]. Many solar problems including precise modelling of the deep convection zone, understanding the emergent acoustic energy flux and its interaction with chromosphere, characterizing nonthermality effects, and explaining the mechanisms of coronal acoustic heating are still not explored properly. A comprehensive investigation of these collective helioseismic modes in nonthermal plasma conditions could offer us a new window to delve into the mysterious features of the Sun.

Spicules are high-energetic dynamic jet-like structures that erupt from the solar photosphere and extend through the chromosphere into the lower corona[19–21]. They exhibit transverse oscillations and play vital roles to transport mass and energy into the corona and solar wind. Despite extensive research, the exact mechanisms underlying their origin and dynamics remain unresolved. Transverse Alfvénic fluctuations and horizontal magnetic flux tube motions have been considered a promising energy carrier to the spicules[21]. A good number of recent research reports[21–23] have speculated that the photospheric *p*-mode oscillations may also drive the spicules via mode conversion mechanism. This longitudinal-to-transverse mode conversion occurs near the equipartition region (in chromosphere) where the normal acoustic (longitudinal) speed and normal Alfvén

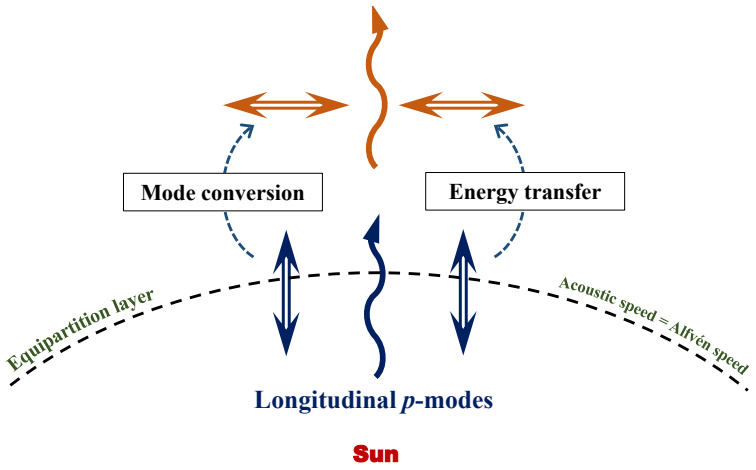


Figure 1. A schematic diagram depicting the mode conversion from longitudinal p-modes to transverse spicule oscillation modes. The black dashed curve represents the equipartition layer formed near the chromosphere.

(transverse) speed become exactly equal. It involves p-mode interaction with magnetic flux tubes that excites both sausage (longitudinal) and kink (transverse) waves[24], allowing energy leakage from the solar interior into the chromosphere. As depicted in Figure 1, this leakage can thereby generate power shocks that further form transverse spicule oscillations[19,21,22]. Key aspects of this wave energy transfer mechanism remain unclear. In this study, we theoretically investigate the acoustic energy flux generated by collective photospheric p-modes and shed some light on the diverse features of the modal energy transformation mechanism that contribute to the chromospheric spicule phenomenon.

Recent space missions—including the Parker Solar Probe (PSP), Solar Terrestrial Relations Observatory (STEREO), and Solar Orbiter (SoLO)—have provided extensive *in situ* observations of the inner heliosphere, offering valuable insights into solar plasma dynamics and heliospheric processes. In addition, space-based observatories such as the Solar and Heliospheric Observatory (SOHO), *Wind*, and the Solar Dynamics Observatory (SDO) have also detected a wide range of wave modes and oscillations on the solar surface. These observations are complemented by ground-based networks, including the Taiwan Oscillation Network (TON), the Global Oscillation Network Group (GONG), and the Birmingham Solar Oscillations Network (BiSON), which together enhance our understanding of solar interior structure, magnetic activity, and energetic particle dynamics[1,5,11,25,26].

It is noteworthy that the space and astrophysical plasmas generally exist in stationary (time invariant) statistical states out of thermal equilibrium, i.e., athermal[28,29]. They often exhibit large-scale inhomogeneities and turbulence due to the presence of free energy sources of diversified origins. Therefore, the Maxwell–Boltzmann distribution becomes inadequate to describe the long-range interactions in the collisionless nonextensive space plasmas with plasma coupling parameter, $\Gamma << 1$. Such non-Maxwellian suprathermal particle velocity distribution is observed ubiquitously in the solar wind[30,31]). Observations from multiple missions unveil that the solar electrons often form suprathermal tails, deviating from Maxwellian distributions due to reduced collisions among faster electrons with longer mean free paths[32,33].

The astrophysical non-Maxwellian (nonthermal) systems are governed by the Tsallis nonextensive statistical mechanics[34]. Since the solar electron distributions have high-energy tails, the distribution function ($f(v)$) often follows an inverse power law $f(v) \propto v^{-x}$, such as the kappa distribution (κ-distribution) function containing the nonthermality spectral index κ[29,32,35,36]. The family of this kappa velocity distribution has been first introduced by[32]. The κ-distribution—extensively known as the q-exponential or the q-Maxwellian distribution—is well-recognized for appropriately modelling the suprathermal constitutive species of space plasmas[29,35–37]. The possible realistic values of the nonthermality spectral index, κ, lie in the range as $3/2 < \kappa \leq \infty$. For $\kappa \to 3/2$, the system approaches the farthest state from the equilibrium, i.e., “anti-equilibrium"; while, for $\kappa \to \infty$, the system reverts to the Maxwell distribution[29,35,36,38].

Viscosity is a key factor to define the solar plasma dynamics, as it influences the momentum and energy transformation within the fluid. Its effect in the solar plasma has been first studied by Noble and Scarf[39]. Later, Whang *et al.*[40] have observed that the viscosity acts as an energy dissipative source in the interplanetary medium, reducing both heat flow and the system’s total energy. Several recent reports have considered the solar plasmas as viscous fluid to describe its dynamics[41,42]. Therefore, the viscosity effect must be sincerely incorporated in order to conduct a proper investigation of the solar plasma dynamics.

In this theoretical work, we systematically investigate the collective waves and oscillation features over the κ-distributed solar interior plasma model. The novelty of our analyses lies in the systematic incorporation of the conjoint action of fluid

viscosity and thermal conductivity along with the nonthermal electron distribution effect to study the entire solar plasma spatiotemporal regime. Here, our main focus is to see the non-trivial effects of the constitutive suprathermal electrons on the helioseismic modes elaborately. Besides, we critically analyse diverse characteristics of the g-mode and p-mode in conformity with the existing numerous observational scenarios. It is clearly obtained from our report that the effects of nonthermality, electron temperature, thermal conductivity, and fluid viscosity play significant role in the wave propagation dynamics on the solar interior plasma regimes.

The structural layout of this manuscript is methodically organized as follows. Apart from the introduction part as in Section 1, the model configuration and formalism details are offered in Section 2. The kappa-distributed parametric fluctuation features in the solar interior regime are described in Subsection 2.1. Section 3 is devoted to discuss the stability criteria analysis of the entire solar plasma dynamics by applying the Routh–Hurwitz (R-H) criterion. In Section 4, we depict the main results and discussions along with a reliability comparison and validation analysis with the astronomical solar observations reported extensively in the literature. The main conclusions drawn from our systematic investigation, together with futuristic scope in the helioseismic direction, are finally highlighted in Section 5.

2 PHYSICAL MODEL FORMALISM

In this semi-analytic study, we consider an inhomogeneous nonthermal solar plasma model that is quasi-neutral, viscoturbulent (viscous + turbulent), and thermally conductive. Within the self-gravitating solar interior, the thermal plasma pressure ($p_t = nk_{\rm B}T$) significantly dominates over magnetic pressure ($p_m = B^2/2\mu_0$) and hence the plasma β-parameter ($\beta = p_t/p_m$) becomes very high (>> 1)[1,3]. Consequently, the magnetic field exerts negligible effects on the collective helioseismic modes[43–46]. Therefore, magnetic field effects are excluded herein to isolate the dependence of modal features on the underlying physical properties of the adopted solar model. For a reasonable approximation, the Sun is assumed to be spherically symmetric, thereby ignoring the effects of rotation and magnetic field. It comprises mainly of suprathermal (inertialess) electrons and non-isothermal (inertial) ions. This solar plasma itself originates from the thermonuclear fusion of its primary constituents: Hydrogen (92%) and Helium (8%)[1,3,8,26]. The lighter unbounded electrons are treated as nonthermal (κ-distributed) particles, whereas, the heavier bounded ions are considered as an inhomogeneous non-isothermal inertial fluid.

In this adopted model, plasma turbulence—causing outward irregularities in pressure and velocity—and fluid viscosity—offering inward resistance to flow—are carefully incorporated[40,47]. Owing to the dominance of plasma pressure over magnetic pressure, the solar interior is typically approximated as magnetic field-free and modelled as a polytrope. The polytropic equation of state (EoS) for the effective plasma fluid pressure with density $\rho(r)$ is given as $p(r) = K_p\rho(r)^{\gamma_p} = K_p\rho(r)^{\left(1+n_p^{-1}\right)}$; where, K_p is the polytropic constant, $\gamma_p = \left(1+n_p^{-1}\right)$ denotes the polytropic exponent, and $n_p = \left(\gamma_p - 1\right)^{-1}$ implies the polytropic index[7,8,48]. For a special case of isothermal condition, $\gamma_p = 1$ and hence, the corresponding isothermal homogeneous fluid pressure becomes $p_{\rm th} = nk_{\rm B}T_{\rm th}$; where, $T_{\rm th}$ is the homogeneous ($\partial_r T_{\rm th} = 0$) time-invariant ($\partial_t T_{\rm th} = 0$) fluid temperature (in K) and n denotes the constituent particle number density. $k_{\rm B}$ refers to the Boltzmann constant, physically signifying the temperature-energy conversion factor ($k_{\rm B} = 1.38\times10^{-23}\,{\rm J\,K^{-1}}$). In this adopted inhomogeneous solar plasma configuration, the non-isothermal ionic fluid pressure is given as $p_s(r,t) = n_i(r,t)k_{\rm B}T_i(r,t)$; where, $T_i(r,t)$ is the inhomogeneous ($\partial_r T_i \neq 0$) time-variant ($\partial_t T_i \neq 0$) fluid temperature and $n_i(r,t)$ denotes the inhomogeneous time-variant ion number density.

Inhomogeneities in solar plasma—specifically density and temperature gradients—give rise to the turbulence pressure in the system[1,26]. The active isotropic fluid turbulence pressure is modelled by the Larson logabarotropic EoS: $p_{\rm turb} = p_0\ln\{\rho(r,t)/\rho_0\}$; where, $p_0 = n_0k_{\rm B}T_0$ is the mean (equilibrium) isothermal fluid pressure, $\rho(r,t)$ refers to the inhomogeneous fluid material volumetric density, and ρ_0 denotes the mean the mean solar fluid density[47,49,50]. The net pressure of the non-isothermal inhomogeneous turbulent solar plasma ionic fluid is thus $p = (p_s + p_{\rm turb})$. For mathematical tractability, effects such as the heliospheric magnetic field (HMF), gyro-fluid interaction, non-ideality, differential rotation, vorticity, viscoelasticity, bulk viscosity, and tidal forces are neglected.

For our semi-analytic investigations, we adopt standard notations and typical values of key physical parameters relevant to solar plasma dynamics[1,3,26], as listed in Table 1. A standard Jeans normalization scheme[1,3,5,45,46,51], adopted in the present astrophysical analysis along with the corresponding definitions of variables and characteristic solar plasma scales, is summarized in Table 2. The adoption of Jeans normalization is primarily motivated by the need to consistently incorporate self-gravitational effects into the plasma-fluid description of the Sun. The Sun is believed to have originated through the gravitational collapse of primordial matter resulting from density inhomogeneities, a process fundamentally associated with Jeans instability. Even after its formation, the Sun remains a self-gravitating system whose structure and evolution are governed by the interplay between gravitational and thermodynamic processes. The associated Jeans length and Jeans time scales characterize the balance between pressure-driven restoring forces and gravitational attraction, thereby providing a physically meaningful framework for nondimensionalizing the governing equations of a self-gravitating plasma medium. Furthermore, the use of Jeans normalization enables the fundamental role of gravity in large-scale plasma dynamics to be incorporated in a natural and self-consistent

Table 1. Representative solar physical parameters

Physical parameter	Symbol	Magnitude
Electron mass	m_e	$9.31\times10^{-31}\,\mathrm{kg}$
Ion (proton) mass	m_i	$1.67\times10^{-27}\,\mathrm{kg}$
Electron charge	$q_e=-e$	$-1.6\times10^{-19}\,\mathrm{C}$
Ion (proton) charge	$q_i=+e$	$+1.6\times10^{-19}\,\mathrm{C}$
Electron temperature	T_e	$10^6\,\mathrm{K}\,(\approx10^2\,\mathrm{eV})$
Ion temperature	T_i	$10^5\,\mathrm{K}\,(\approx10\,\mathrm{eV})$
Solar core temperature	T_c	$10^7\,\mathrm{K}\,(\approx10^3\,\mathrm{eV})$
Boltzmann constant	k_B	$1.38\times10^{-23}\,\mathrm{J\,K^{-1}}$
Vacuum permittivity	ε_0	$8.85\times10^{-12}\,\mathrm{C^2\,kg^{-1}\,m^{-3}\,s^2}$
Vacuum permeability	μ_0	$4\pi\times10^{-7}\,\mathrm{kg\,m\,s^{-2}\,A^{-2}}$
Universal gravitational constant	G	$6.67\times10^{-11}\,\mathrm{m^3\,kg^{-1}\,s^{-2}}$

Table 2. Adopted astrophysical normalization scheme

Normalized parameter	Normalizing parameter	Magnitude
Radial distance $\left(\xi=\frac{r}{\lambda_\mathrm{J}}\right)$	Jeans length (λ_J)	$3.1\times10^8\,\mathrm{m}$
Time $\left(\tau=\frac{t}{\tau_\mathrm{J}}\right)$	Jeans time $\left(\tau_\mathrm{J}=\omega_\mathrm{J}^{-1}\right)$	$10^3\,\mathrm{s}$
Population density $\left(N_{e(i)}=\frac{n_{e(i)}}{n_0}\right)$	Mean SIP density (n_0)	$10^{30}\,\mathrm{m^{-3}}$
Mach number $\left(M=\frac{v_{(i)}}{C_s}\right)$	Sound phase speed (C_s)	$3.1\times10^5\,\mathrm{m\,s^{-1}}$
Gravitational potential $\left(\Psi=\frac{\psi}{C_s^2}\right)$	Sound speed squared $\left(C_s^2\right)$	$9.61\times10^{10}\,\mathrm{m^2\,s^{-2}}$
Electrostatic potential $\left(\Phi=\frac{e\phi}{k_\mathrm{B}T_e}\right)$	Thermal potential $\left(\frac{k_\mathrm{B}T_e}{e}\right)$	$10^2\,\mathrm{J\,C^{-1}}$

manner. It is noteworthy that the Sun itself serves as a standard normalization reference in astrophysics through quantities such as the solar mass, solar radius, and solar luminosity, which are widely employed to describe the properties and evolutionary behavior of other stellar systems in a scale-invariant framework[1,3].

Although the solar plasma is intrinsically stratified, the present formulation employs a local approximation in which background variations are assumed to be weak over the perturbation scale. Within this regime, the Jeans scaling offers an effective normalization to capture the coupled effects of compressibility, nonthermality, and dissipation, without explicitly resolving the global stratification of the Sun.

2.1 Nonthermal solar plasma fluctuations

This work aims to study the solar plasma fluctuation dynamics in the presence of fluid viscosity, turbulence, thermal conductivity, and nonthermal kappa (κ) spectral effects. The suprathermal (athermal) electron population density obeys the relevant nonthermal power-law of population distribution[29,35,36,52,53]. Accordingly, the electron thermostatistical distribution law in the normalized form with all the customary notations is given as

$$N_e=N=\left[1-\Phi\,(\kappa-3/2)^{-1}\right]^{-\kappa+1/2}. \tag{1}$$

Here, the solar plasma quasi-neutrality condition, $N_e\approx N_i=N$, is a direct natural consequence of the electrostatic Poisson equation on the gravitational Jeans spatial scales, $\lambda_\mathrm{J}\to\infty$, against the electrostatic Debye screening scales, $\lambda_\mathrm{D}\to0$ such that

$\lambda_D/\lambda_J \approx 10^{-20} \sim 0$ asymptotically[54,55]. The symbol, κ, denotes the nonthermality spectral index measuring the degree of nonthermality (non-extensivity) of the solar suprathermal electrons.

The evolutionary dynamics of the constitutive ions in the self-gravitating solar plasma system can be well described by the full inertial response in the continuum framework of viscoturbulent fluid. The normalized ion hydrodynamic equations including continuity (material density conservation), momentum (force density conservation), and the plasma heat flow (energy conservation) equations can be described in the assumed spherical symmetry (polar and azimuthal contributions ignored) with all the customary notations (Table 1) respectively as

$$\partial_\tau N + N\partial_\xi M + M\partial_\xi N + (2/\xi)MN = 0, \tag{2}$$

$$N\left(\partial_\tau M + M\partial_\xi M\right) + \epsilon_{T_0}\partial_\xi P_N + N\partial_\xi \Phi + N g_s = \eta_{\text{eff}}\left[\partial_\xi^2 M + (2/\xi)\,\partial_\xi M - \left(2/\xi^2\right)M\right], \tag{3}$$

$$\left(\partial_\tau P_N + M\partial_\xi P_N\right) + \gamma\, P_s\left[\partial_\xi M + (2/\xi)M\right] - (\gamma-1)\,\kappa^*_{\text{Th}}\left[\partial_\xi^2 T_N + (2/\xi)\,\partial_\xi T_N\right] = Q(\gamma-1)/(p_0\Omega_J). \tag{4}$$

Here, $\partial_{\tau(\xi)}$ denotes the linear partial differential operator with respect to Jeans-normalized time (radial space). Then, $P_N(\xi,\tau) = [P_s(\xi,\tau) + P_{\text{turb}}(\xi,\tau)] = [N(\xi,\tau)T_N(\xi,\tau) + \ln\{N(\xi,\tau)\}]$ stands for the total (non-isothermal + turbulent) effective normalized pressure of the considered inhomogeneous solar plasma system lying initially in a hydrostatic homogenous quasi-neutral equilibrium configuration. ${\epsilon_{T_0}}^{-1} = T_e/T_0$ and $T_N = T_i/T_0$ represent the normalized electron and ion temperatures, respectively. T_0 is the solar mean (equilibrium) temperature (in K), treated as the temperature normalizing parameter. Φ denotes the normalized electrostatic potential in the plasma. $g_s = \partial_\xi \Psi$ implies the Jeans-normalized self-gravitational acceleration; where, Ψ denotes the Jeans-normalized self-gravitational potential.

Clearly, Equation (3) represents the Navier–Stokes equation, with only dynamic (shear) viscous effect, but with no bulk viscous effects. The dimensionless (normalized) parameter, $\eta_{\text{eff}} = \eta/\left(m_i n_0 \omega_J \lambda_J^2\right)$, denote the coefficients of effective dynamic (shear) viscosity arising because of the collisional energy exchange processes among the constitutive ionic species. Here, the viscosity normalizing parameter is the Jeans (critical) viscosity, given as $\eta_J = m_i n_0 \omega_J \lambda_J^2$. The notation, η, represents the zeroth-order dynamic viscosity coefficient of the plasma ion fluid and can be given with all the usual notations as $\eta = 0.96 n_i k_B T_i t_r$ (in kg m^{-1} s^{-1} or Pa s); where, $t_r = 12\pi^{3/2}{\varepsilon_0}^2 m_i^{1/2} e^{-4}(\ln\Lambda)^{-1} n_i^{-1}(k_B T_i)^{3/2}$ (in seconds) refers to the typical Coulombic relaxation time for the solar ions[42,56,57]. The parameter, ϵ_0, denotes the vacuum permittivity. The logarithmic notation, $\ln\Lambda$, denotes the Coulomb logarithm that reflects the dominance of small-angle over large-angle Coulomb collisions.

As in Equation (4), the dimensionless (normalized) parameter, $\kappa^*_{\text{Th}} = \kappa_{\text{Th}}/\left(n_0 k_B \omega_J \lambda_J^2\right)$, stands for the coefficient of effective thermal conductivity arising because of the thermal energy exchange processes among the constitutive ions. Here, the conductivity normalizing parameter is the Jeans (critical) thermal conductivity, given as $\kappa_{\text{ThJ}} = n_0 k_B \omega_J \lambda_J^2$. The notation, κ_{Th}, denotes the zeroth-order thermal conductivity of the considered plasma system. It can be given in the usual notations as $\kappa_{\text{Th}} = 3.9 n_i k_B^2 T_i t_r m_i^{-1}$ (in kg m s^{-3} K^{-1} or W m^{-1} K^{-1})[56,57]. The thermodynamic term, $Q = \vec{\nabla}\cdot\vec{q}$, represents the divergence of effective heat flux defining the heat source type (outward flux, $Q > 0$) or sink type (inward flux, $Q < 0$) characteristic of the solar plasmas. The notation, γ, denotes the well-known specific heat ratio that can be obtained as $\gamma = 5/3$ for the considered singly ionized solar plasmas.

The self-gravitational Poisson equation describing the gravitational potential distribution caused by the gravitating plasma density fields[1,3]) finally closes the system as

$$\partial_\xi g_s + (2/\xi)\, g_s = \left[1 - \Phi(\kappa - 3/2)^{-1}\right]^{-\kappa+1/2}. \tag{5}$$

The Jeans-normalized solar self-gravity is denoted as $g_s = \partial_\xi \Psi$. The $(2/\xi)$-term appears in all of the governing equations due to the "geometrical curvature effect" which arises as we consider the spherical geometry ($\xi \twoheadrightarrow \infty$) configuration to define our model.

2.1.1 Linear stability analysis

A local linear normal mode perturbation analysis is employed to study the collective wave and oscillation features on the entire solar plasma regime relative to its defined hydrostatic homogeneous equilibrium. Accordingly, the Eulerian perturbation treatment is applied systematically. We denote the equilibrium quantities (homogenous, static) with subscript "0" and the corresponding linear (1$^{\text{st}}$ order) perturbation (inhomogenous, non-static) with subscript "1", given parametrically in an explicit mathematical form as

$$\begin{pmatrix} N \\ M \\ \Phi \\ g_s \\ T_N \end{pmatrix}(\xi,\tau) = \begin{pmatrix} N_0 \\ M_0 \\ \Phi_0 \\ g_{s0} \\ T_{N0} \end{pmatrix} + \begin{pmatrix} N_1 \\ M_1 \\ \Phi_1 \\ g_{s1} \\ T_{N1} \end{pmatrix}(\xi,\tau). \tag{6}$$

Here, the local equilibrium values of the relevant physical parameters are given as $N_0 = 1$, $M_0 = 0$, $\Phi_0 = 0$, $g_{s0} = 0$, and $T_{N0} = 1$. Accordingly, the linearized perturbed forms of the governing equations (Equations (1)-(5)) can be respectively cast as

$$N_1 = \alpha\Phi_1, \tag{7}$$

$$\partial_\tau\Phi_1 + \alpha^{-1}\left[\partial_\xi M_1 + (2/\xi)M_1\right] = 0, \tag{8}$$

$$\partial_\tau M_1 = -\epsilon_{T_0}\partial_\xi T_{N1} - \left(1 + 2\epsilon_{T_0}\alpha\right)\partial_\xi\Phi_1 - g_{s1} + \eta_{\text{eff}}\left[\partial_\xi^2 M_1 + (2/\xi)\partial_\xi M_1 - \left(2/\xi^2\right)M_1\right], \tag{9}$$

$$\partial_\tau T_{N1} + 2\alpha\partial_\tau\Phi_1 + \gamma\left[\partial_\xi M_1 + (2/\xi)M_1\right] - (\gamma-1)\kappa^*_{\text{Th}}\left[\partial_\xi^2 T_{N1} + (2/\xi)\partial_\xi T_{N1}\right] = 0, \tag{10}$$

$$\partial_\xi g_{s1} + (2/\xi)g_{s1} = \alpha\Phi_1. \tag{11}$$

Now, we assume an infinitesimal perturbation is growing homologously in the form of spherically symmetric (radial dependency) waves defined in a generalized form for all the perturbed solar parameter as $F_1(\xi,\tau) \sim (1/\xi)\exp[-i(\Omega\tau - K\xi)]$. Here, such perturbation is also referred to as the Eulerian perturbation at a given spatiotemporal point[5]. The considered spherically symmetric perturbations enable us to get rid of the polar and azimuthal contributions in the same model. $\Omega = \omega/\omega_{\text{J}}$ and $K = k/k_{\text{J}}$ are the Jeans-normalized angular frequency and the Jeans-normalized angular wavenumber of the considered local linear perturbation, respectively. Now, operating linear spatiotemporal differentiation on F_1 enables us to transform the direct coordination space (ξ,τ) into the Fourier (inverse) space (K,Ω), given with the linear Fourier operator transformations as $\partial_\tau \to (-i\Omega)$, $\partial_\xi \to (iK - 1/\xi)$, and $\partial_\xi^2 \to \left(2/\xi^2 - K^2 - 2iK/\xi\right)$. It transforms the linearized equations (Equations (7)–(11)) into the corresponding algebraic forms, cast respectively as

$$M_1 = i\alpha\Omega(iK + 1/\xi\,)^{-1}\Phi_1, \tag{12}$$

$$\left[i\Omega - \eta_{\text{eff}}\left(K^2 + 2/\xi^2\right)\right]M_1 = (iK - 1/\xi)\epsilon_{T_0}T_{N1} + \left(1 + 2\epsilon_{T_0}\alpha\right)(iK - 1/\xi)\Phi_1 + g_{s1}, \tag{13}$$

$$T_{N1} = i\alpha\Omega(2-\gamma)\left[(\gamma-1)\kappa^*_{\text{Th}}K^2 - i\Omega\right]^{-1}\Phi_1, \tag{14}$$

$$g_{s1} = \alpha(iK + 1/\xi)^{-1}\Phi_1. \tag{15}$$

Now, substituting Equations (12), (14), and (15) in Equation (13), we get the following generalized linear cubic dispersion relation for the solar plasma fluctuations as

$$A_3\Omega^3 + A_2\Omega^2 + A_1\Omega + A_0 = 0; \tag{16}$$

$$A_3 = 1, \tag{17}$$

$$A_2 = i\left[\eta_{\text{eff}}\left(K^2 + 2/\xi^2\right) + (\gamma - 1)\kappa^*_{Th}K^2\right], \tag{18}$$

$$A_1 = \left[1 - (\gamma - 1)\eta_{\text{eff}}\kappa^*_{\text{Th}}K^2\left(K^2 + 2/\xi^2\right) - \left(\gamma\epsilon_{T_0} + \alpha^{-1}\right)\left(K^2 + \xi^{-2}\right)\right], \tag{19}$$

$$A_0 = i(\gamma - 1)\left[1 - \left(2\epsilon_{T_0} + \alpha^{-1}\right)\left(K^2 + \xi^{-2}\right)\right]\kappa^*_{\text{Th}}K^2. \tag{20}$$

Equation (16) provides a local approximation-based description of solar (in)stability dynamics relative to the equilibrium state. The notation, $\alpha = (2\kappa - 1)/(2\kappa - 3)$, emerges as a thermostatistical index, capturing the deviation of solar plasma behaviour from the classical Boltzmann–Gibbs extensivity. Analytically, it is evident that the modal dispersion features are governed by the interplay of several effects, such as geometrical curvature (via A_0, A_1, and A_2), viscoturbulence (via A_1 and A_2), thermal conductivity (via A_0, A_1, and A_2), thermo-plasmicity (via A_0 and A_1), and plasma nonthermality (via A_0 and A_1). Apart from the above, the inner details of the plasma multi-parametric dependencies of the helioseismic dispersion behaviours can be explicitly analysed through the functional windows of the diverse dispersion coefficients expressed with Equations (17)-(20). Overall, the obtained cubic dispersion relation expressed by Equation (16) encapsulates the diverse behaviors of the fundamental helioseismic (g- and p-)modes.

3 STABILITY CRITERIA ANALYSIS

Let us now analyse the dynamical stability of the nonthermal κ-modified solar plasma system using the Routh–Hurwitz (R-H) criterion[58]. Guillemin[59] has identified the necessary and sufficient conditions under which any polynomial becomes a Hurwitz polynomial. According to the Guillemin criterion, for any polynomial to be a Hurwitz one, all the involved coefficients of the given polynomial should necessarily be positive. In a characteristic equation, if any coefficient is zero or if any coefficient is negative, then at least one root has a zero or positive real part, indicating the system to be neutrally stable or unstable, respectively. While, the positive coefficients—denoting a Hurwitz—are necessary, they alone do not provide a sufficient condition for stability.

When this condition is met, system stability is assessed by constructing an array called Routh array from the coefficients of the Hurwitz polynomial. According to the Routh–Hurwitz (R-H) criterion, the number of roots of the characteristic equation with positive real parts (unstable) is equal to the number of sign changes in the first column of the Routh array[60]. Thus, for a system to be stable, all the involved dispersion coefficients in the first column must have the same sign.

Substituting $\Omega = i\sigma$ in Equation (16), we obtain the characteristic equation of the system as

$$a_3\sigma^3 + a_2\sigma^2 + a_1\sigma + a_0 = 0; \tag{21}$$

$$a_3 = 1, \tag{22}$$

$$a_2 = \left[\eta_{\text{eff}}\left(K^2 + 2/\xi^2\right) + (\gamma - 1)\kappa^*_{\text{Th}}K^2\right], \tag{23}$$

$$a_1 = -\left[1 - (\gamma - 1)\eta_{\text{eff}}\kappa^*_{\text{Th}}K^2\left(K^2 + 2/\xi^2\right) - \left(\gamma\epsilon_{T_0} + \alpha^{-1}\right)\left(K^2 + \xi^{-2}\right)\right], \tag{24}$$

$$a_0 = -(\gamma - 1)\left[1 - \left(2\epsilon_{T_0} + \alpha^{-1}\right)\left(K^2 + \xi^{-2}\right)\right]\kappa^*_{\text{Th}}K^2. \tag{25}$$

Equation (21) is a polynomial in σ, representing the same general dispersion relation for the considered system as expressed earlier in Equation (16), but in an alternative algebraic form.

It is noteworthy that, if $\left(2\epsilon_{T_0} + \alpha^{-1}\right)\left(K^2 + \xi^{-2}\right) > 1$, all the coefficients of Equation (21), given in Equations (22)-(25), become positive. Thereby, it represents a Hurwitz polynomial satisfying the necessary condition for stability of the system.

Table 3. Routh array

$\sigma^3:$	a_3	a_1	0
$\sigma^2:$	a_2	a_0	0
$\sigma^1:$	u_1	u_2	u_3
$\sigma^0:$	v_1	v_2	v_3

In order to investigate the (in)stability criteria of the system, the Routh array is constructed and shown in Table 3. Here, the elements of the third and fourth rows are constructed as

$u_1 = -(a_0a_3 - a_1a_2)/a_2; u_2 = 0; u_3 = 0.$
$v_1 = -(a_2u_2 - a_0u_1)/u_1 = a_0; v_2 = -(a_2u_3 - 0)/u_1; v_3 = 0.$

As $a_3 = 1 (> 0)$, in order to satisfy the sufficient condition for stability, a_2, u_1, and v_1 should be positive. For this, the considered system should obey the inequality given as $\left(2\epsilon_{T_0} + \alpha^{-1}\right)\left(K^2 + \xi^{-2}\right) > 1$. Using all the judicious values of the solar parameters, such as $\epsilon_{T_0} = 0.1$, $\kappa = 2$, we calculate and find the stability criterion for the self-gravitating solar spatiotemporal regime as $(K^2 + \xi^{-2}) > 2$. Hence, putting $\xi = 2.25$ (solar surface), we can analytically predict that, for $K > 1.4$, the nonthermal viscoturbulent inhomogeneous solar surface region becomes stable. Thus, the R-H criterion provides a unique way to find the solar plasma stability condition.

4 RESULTS AND DISCUSSIONS

A systematic numerical analysis, based on normal-mode analysis of the governing hydrodynamic equations, yields a generalized cubic dispersion relation (Equations (16)) that characterizes the κ-modified helioseismic modes in the self-gravitating solar interior plasma. The solution of this dispersion relation produces three roots; among these, the physically relevant branch corresponding to nonthermal fluctuations is analysed in detail. The resulting dynamical features of the coupled solar plasma system are illustrated through colour-spectral profiles in Figures 2–16.

4.1 Nonthermal solar plasma stability features

Using suitable input values, we perform a detailed numerical analysis to examine the stability characteristics of the system. Figure 2 presents 3D profile of the Jeans-normalized angular real frequency part Ω_r as a function of the Jeans-normalized radial distance ξ and Jeans-normalized angular wavenumber K, describing the dynamics of nonthermal helioseismic fluctuations. A magnified view is shown in the right panel. The adopted parameters are $\eta_{\text{eff}} = 0$, $\kappa^*_{\text{Th}} = 0$, $\kappa = 2$, $\epsilon_{T_0} = 0.1$, and $\gamma = 5/3$. The results reveal that the collective waves exhibit strongly dispersive nature at ultra-low ξ-values. An asymptotic trend emerges near $\xi = 0$ (the heliocentre), suggesting a singularity-like nature at the heliocentre. At the surface ($\xi = 2.25$), no propagation is observed for very long gravitational-like waves with $0 < K < 1.4$. It thereby concretizes the fact that the solar internal longer waves with lower Ω_r, known as the "gravity modes" (g-modes), are confined to the solar interior and cannot propagate to the surface. Moreover, for small K-values, the waves are dispersive, while increasing K leads to non-dispersive behaviour. Beyond the heliocentre, the waves frequency shows negligible ξ-dependency at fixed K.

Figure 3 portrays the colourspectral profile of the Jeans-normalized imaginary angular imaginary frequency part Ω_i as a function of the Jeans-normalized radial distance ξ and the Jeans-normalized angular wavenumber K. A zoomed-in view is shown in right panel. The imaginary component of the frequency governs the growth ($\Omega_i > 0$, destabilizing) or decay ($\Omega_i < 0$, stabilizing) of wave amplitude, indicating the (in)stability of helioseismic modes. Near the heliocentre, $\Omega_i \approx 0$ across all K, indicating purely oscillatory modes without any growing nature of instability and a metastable state of the heliocentre. Beyond $\xi \gtrsim 1$, the long-wavelength modes (low-K) exhibit strong growth rates, indicating gravitationally instability within the solar interior. This behaviour is consistent with the well-established picture that buoyancy-driven g-modes are trapped within the radiative zone and do not propagate to the outer layers.

In Figure 4, we illustrate the profiles of the Jeans-normalized real frequency part Ω_r and imaginary frequency part Ω_i as functions of K for different indicated values of the nonthermality spectral index κ at the solar surface ($\xi = 2.25$). The propagation frequency of the collective waves increases as κ enhance, indicating that κ acts as an accelerating parameter. Simultaneously, the growth rate decreases with increasing κ, demonstrating its stabilizing influences. Thus, as the system transitions from a strongly nonthermal state ($\kappa = 2$) toward a near-thermal state ($\kappa \gg 1$), the waves become more propagatory and the system more stable. For $\kappa = 2$, the system shows stable characteristics for $K > 1.4$. Modes with $K \in [0, 1.4]$ do not propagate at the surface,

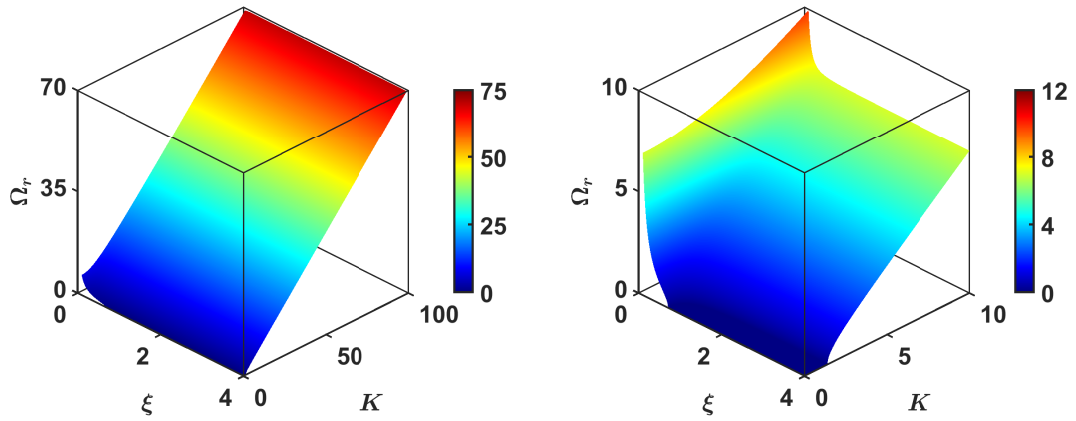


Figure 2. Colourspectral profile of the Jeans-normalized angular real frequency (Ω_r) as a function of Jeans-normalized radial distance (ξ) and the Jeans-normalized angular wavenumber (K) associated with the nonthermal solar plasma fluctuations. A zoomed-in view is shown in the right panel.

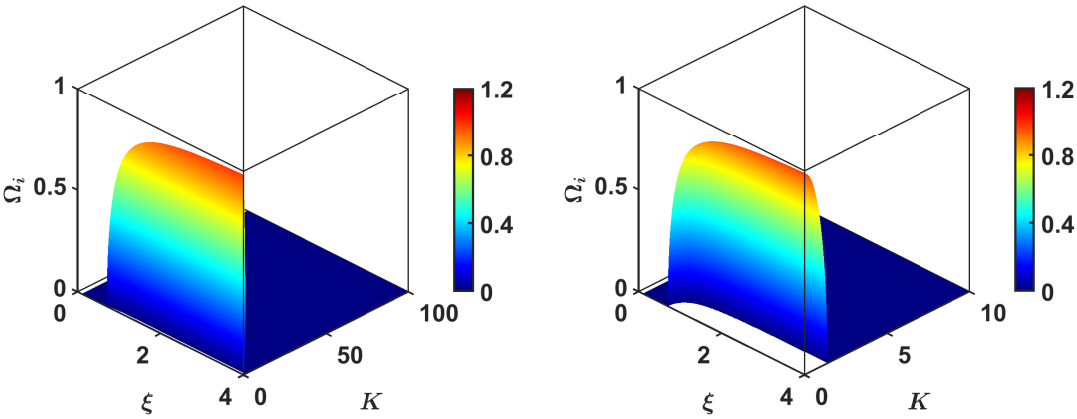


Figure 3. Colourspectral profile of the Jeans-normalized angular imaginary frequency (Ω_i) as a function of Jeans-normalized radial distance (ξ) and the Jeans-normalized angular wavenumber (K) associated with the nonthermal solar plasma fluctuations. A zoomed-in view is shown in the right panel.

confirming their gravitational (g-mode) nature and confinement within the solar interior.

Figure 5 presents similar profiles for different indicated values of the solar equilibrium-to-electron temperature ratio ϵ_{T_0}. Actually, ϵ_{T_0} conveys the reciprocal effect of normalized electron temperature. Increasing ϵ_{T_0} significantly enhances the propagation frequency Ω_r, while simultaneously reducing the growth rate Ω_i. Thus, ϵ_{T_0} acts both as an accelerating and stabilizing parameter. It reveals that the electron temperature induces decelerating and destabilizing effects on the helioseismic modes.

Figure 6 depicts similar profiles for different indicated values of effective shear viscosity η_{eff}. With increasing viscosity, the waves become less propagatory due to enhanced energy dissipation. The growth rate decreases significantly with increasing η_{eff}, indicating that viscosity acts as both a decelerating and stabilizing agent. This behaviour is consistent with viscous damping in fluid systems.

In Figures 7–9, we extend this analysis across different radial positions, demonstrating that the qualitative behaviour remains consistent throughout the spatial domain. The nonthermality parameter κ and the temperature parameter ϵ_{T_0} continue to exhibit accelerating and stabilizing effects, whereas viscosity consistently acts as a decelerating and stabilizing mechanism, thereby confirming the robustness of the model across different solar interior regions.

Figure 10 presents the same analysis (as shown in Figure 4) for the deep interior region ($\xi = 0.5$), where long-wavelength gravitational modes are found to propagate more efficiently, while shorter wavelengths exhibit stronger propagatory characteris-

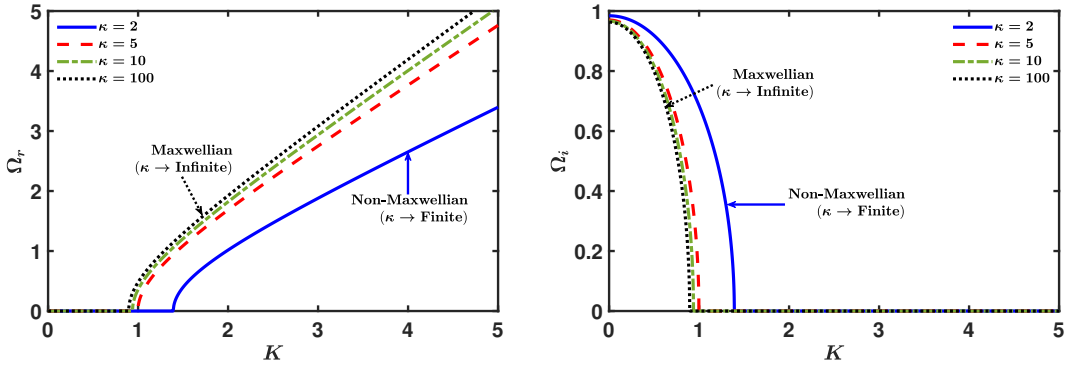


Figure 4. Profiles of the Jeans-normalized angular real frequency (Ω_r) and Jeans-normalized angular imaginary frequency (Ω_i) as functions of the Jeans-normalized angular wavenumber (K) for different values of the nonthermality spectral index (κ) associated with the nonthermal solar plasma fluctuations.

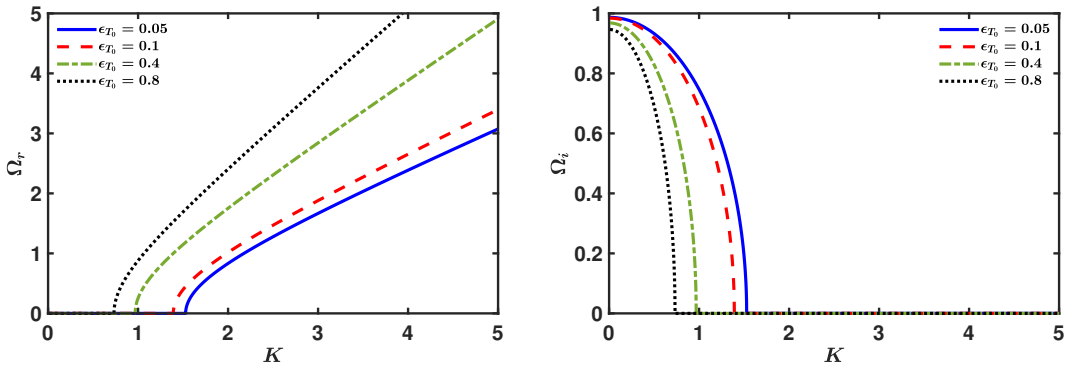


Figure 5. Profiles of the Jeans-normalized angular real frequency (Ω_r) and Jeans-normalized angular imaginary frequency (Ω_i) as functions of the Jeans-normalized angular wavenumber (K) for different values of the solar equilibrium-to-electron temperature ratio (ϵ_{T_0}) associated with the nonthermal solar plasma fluctuations.

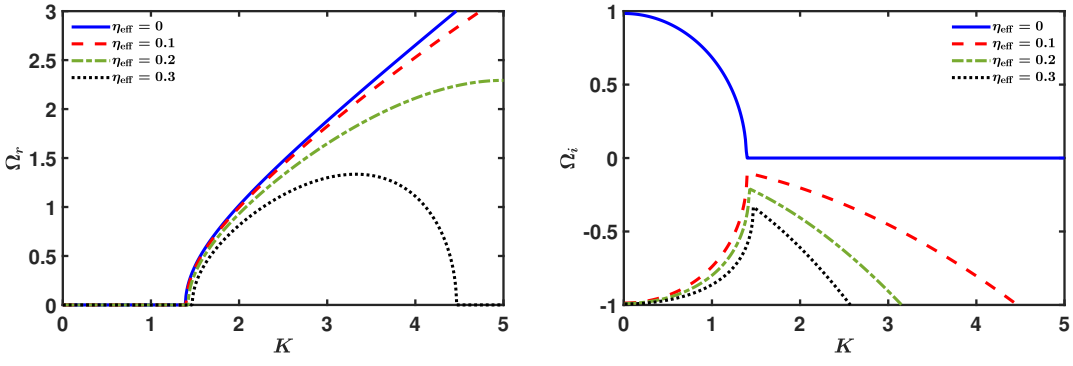


Figure 6. Profiles of the Jeans-normalized angular real frequency (Ω_r) and Jeans-normalized angular imaginary frequency (Ω_i) as functions of the Jeans-normalized angular wavenumber (K) for different values of the effective shear viscosity (η_{eff}) associated with the nonthermal solar plasma fluctuations.

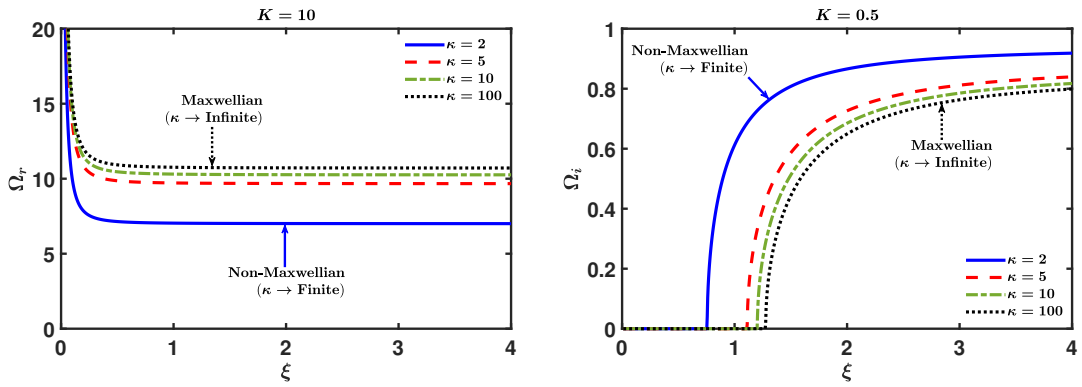


Figure 7. Profiles of the Jeans-normalized angular real frequency (Ω_r) and Jeans-normalized angular imaginary frequency (Ω_i) as functions of the Jeans-normalized radial distance (ξ) for different values of the nonthermality spectral index (κ) associated with the nonthermal solar plasma fluctuations.

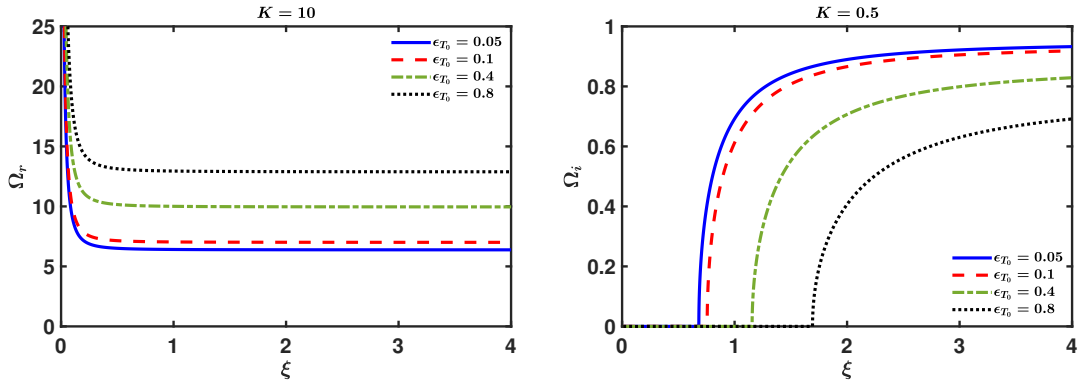


Figure 8. Profiles of the Jeans-normalized angular real frequency (Ω_r) and Jeans-normalized angular imaginary frequency (Ω_i) as functions of the Jeans-normalized radial distance (ξ) for different values of the solar equilibrium-to-electron temperature ratio (ϵ_{T_0}) associated with the nonthermal solar plasma fluctuations.

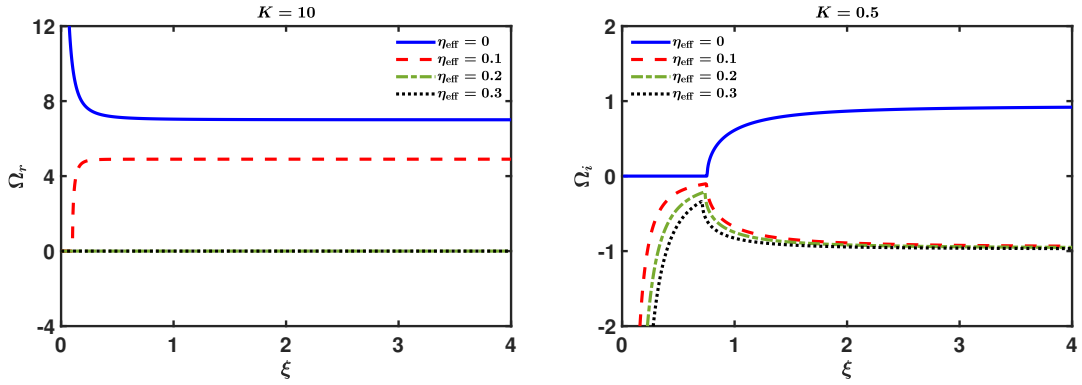


Figure 9. Profiles of the Jeans-normalized angular real frequency (Ω_r) and Jeans-normalized angular imaginary frequency (Ω_i) as functions of the Jeans-normalized radial distance (ξ) for different values of the effective shear viscosity ($\eta_{\rm eff}$) associated with the nonthermal solar plasma fluctuations.

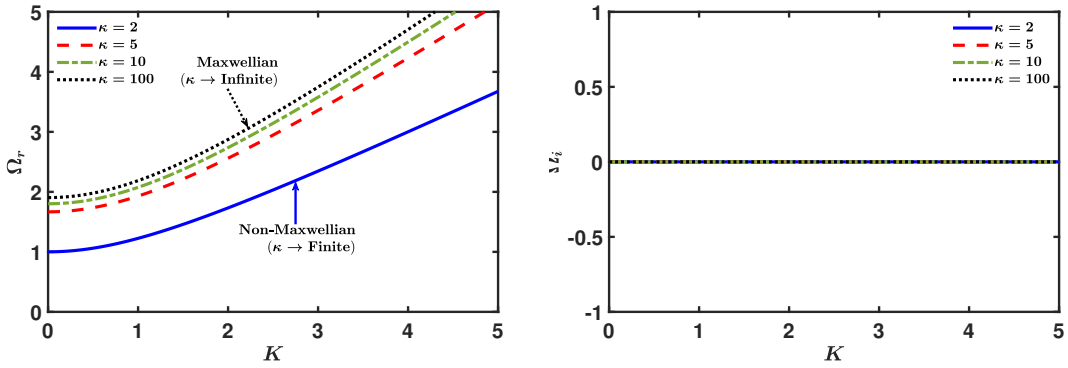


Figure 10. Same as Figure 4, but for the solar interior spatial regime at $\xi = 0.5$.

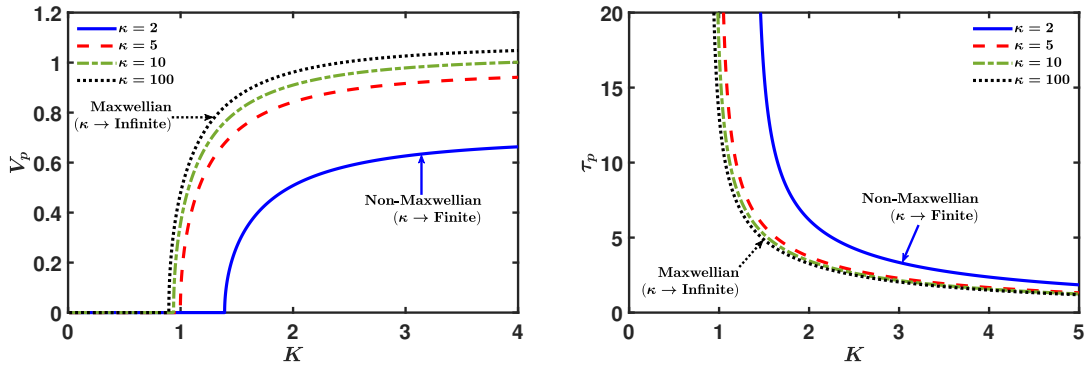


Figure 11. Profiles of the Jeans-normalized phase-velocity (V_p) and Jeans-normalized time period (τ_p) as functions of the Jeans-normalized angular wavenumber (K) for different values of the nonthermality spectral index (κ) associated with the nonthermal solar plasma fluctuations.

tics. In this regime, variation in κ has negligible influence on the growth rate Ω_i, indicating a metastable state dominated by gravitational equilibrium.

Figures 11–13 delineate the profiles of the Jeans-normalized phase velocity V_p and Jeans-normalized time period τ_p as functions of K for different indicated values of the κ-index, ϵ_{T_0}, and η_{eff}, respectively. The phase velocity increases with κ and ϵ_{T_0}, while decreasing with increasing viscosity, indicating that waves propagate faster as the system approaches thermal equilibrium, whereas viscous dissipation reduces the propagation speed. The combined effects of turbulent pressure and self-gravitational confinement further contribute to the reduction of phase velocity. On the other hand, the time period decreases with increasing κ and ϵ_{T_0}, particularly in the long-wavelength regime. Whereas, increasing viscosity leads to a significant increase in the time period, indicating slower oscillations in dissipative environments.

Figure 14 further demonstrates, in the deep interior region ($\xi = 0.5$), the long-wavelength g-modes propagate with higher phase velocity and exhibit longer oscillation periods compared to shorter-wavelength modes.

Figure 15 reveals the temporal evolution of the normalized perturbation (F_1) for various helioseismic modes under the thermal and nonthermal conditions across various spatial depths. The g-mode ($K = 0.5$) displays purely oscillatory behaviour in the deep interior but shows exponential growth near the surface, indicating large-scale instability without effective wave propagation. Conversely, the p-modes ($K = 1.5, 5$) retain their periodic nature with minimal damping as they propagate outward. Shorter-wavelength p-modes oscillate at higher frequencies than longer-wavelength g-modes, consistent with helioseismic theory. Furthermore, thermal plasmas exhibit higher oscillation frequencies compared to nonthermal cases, owing to enhanced effective inertia associated with the larger population of low-energy electrons.

4.2 Helioseismic modal energy flux

We analytically examine the characteristics of the outward radiant energy flux density (f_r) associated with the helioseismic modes in the solar surface regime. The radiant energy flux density of the upward-propagating longitudinal helioseismic modal

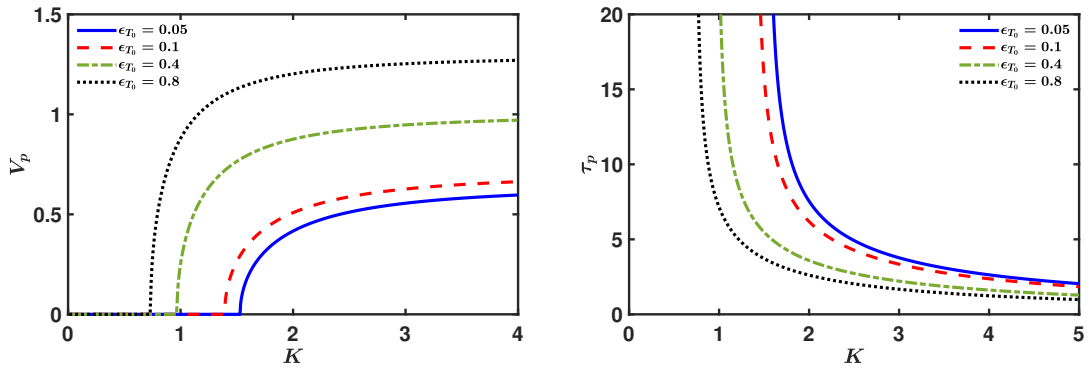


Figure 12. Profiles of the Jeans-normalized phase-velocity (V_p) and Jeans-normalized time period (τ_p) as functions of the Jeans-normalized angular wavenumber (K) for different values of the solar equilibrium-to-electron temperature ratio (ϵ_{T_0}) associated with the nonthermal solar plasma fluctuations.

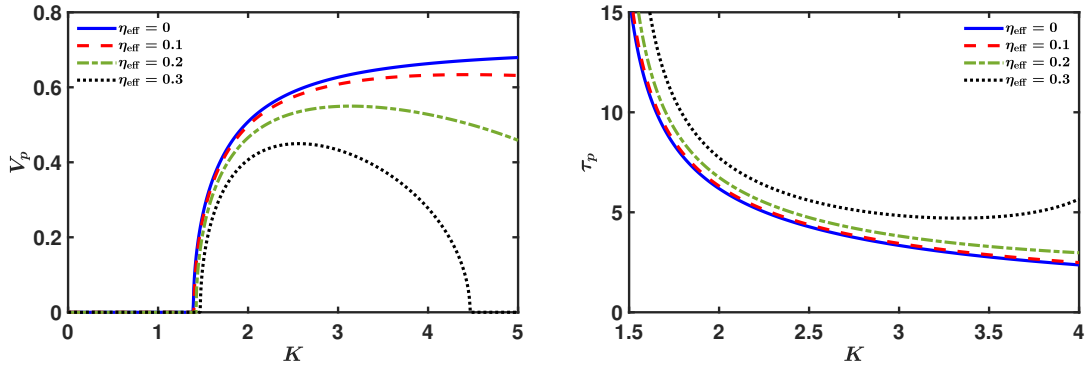


Figure 13. Profiles of the Jeans-normalized phase-velocity (V_p) and Jeans-normalized time period (τ_p) as functions of the Jeans-normalized angular wavenumber (K) for different values of the effective shear viscosity ($\eta_{\rm eff}$) associated with the nonthermal solar plasma fluctuations.

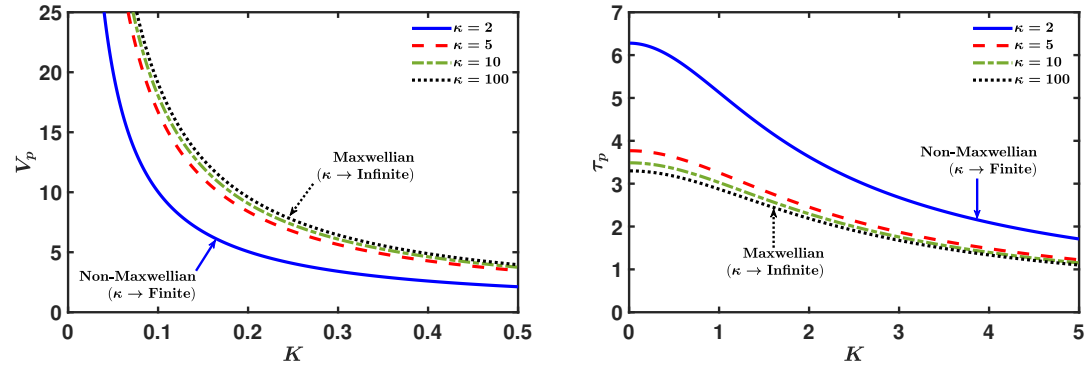


Figure 14. Same as Figure 11, but for the solar interior spatial regime at $\xi = 0.5$.

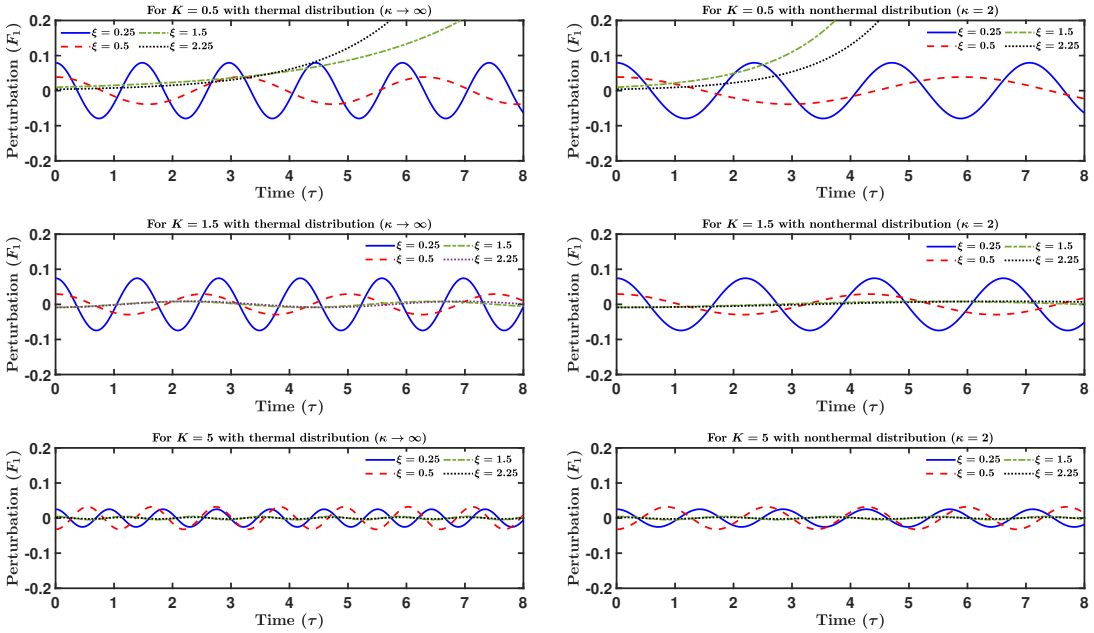


Figure 15. Temporal evolution of normalized perturbation (F_1) as a function of the Jeans-normalized time (τ) for various values of the Jeans-normalized solar radial distance (ξ). The left column illustrates results for the thermal (Maxwellian) distribution, while the right column corresponds to the nonthermal one.

oscillations at the solar surface can be expressed in the unit of W m^{-2} as[22]

$$f_r(\omega, k) = \frac{1}{2}\rho_s v_{p_s} v_r^2, \tag{26}$$

where ρ_s is the local surface fluid density, v_{p_s} denotes the modal phase velocity of radially outward acoustic waves at the surface, and v_r represents the associated velocity amplitude. To nondimensionalize the flux, the Jeans-normalized radiant energy flux density is defined as

$$F_r(\Omega, K) = \frac{f_r}{\rho_0 C_s^3} = \frac{1}{2}\rho^* V_{p_s} V_r^2, \tag{27}$$

where ρ_0 is the mean solar density, $\rho^* = \rho_s/\rho_0$ is the normalized surface density, V_{p_s} is the normalized surface phase velocity, and V_r is the normalized velocity amplitude.

Figure 16 illustrates the profile of F_r as function of K for different values of the κ, ϵ_{T_0}, η_{eff}, and (d) ρ^* at the solar surface ($\xi = 2.25$). Notably, the parameters κ, ϵ_{T_0}, and ρ^* intensify the energy flux radiating outward. In contrast, increasing viscosity leads to a substantial reduction in F_r due to enhanced dissipative losses. These results indicate that nonthermal effects and thermal energy coupling facilitate efficient outward energy transport, while viscous dissipation suppresses it. Near the solar surface, p-modes play a crucial role in radiating energy from the interior resonant cavity into the overlying atmospheric layers. This outward energy transport can trigger the excitation of various wave modes and oscillatory structures in the chromosphere and corona.

The present analysis reveals that the radiant energy flux density lies in the range of $f_r = 10^5 - 10^6$ W m^{-2}. Observational studies[19,20,61] report energy flux values of the order $10^3 - 10^4$ W m^{-2} associated with transverse spicule oscillations. This correspondence strongly suggests that the p-modes possess adequate potential to significantly contribute to spicule formation, likely through partial conversion of longitudinal acoustic energy into transverse wave modes.

Moreover, the results indicate pronounced damping of longitudinal p-modes near the photospheric layer, implying substantial leakage of acoustic energy into the overlying atmosphere. This supports the widely accepted scenario in which photospheric p-mode oscillations supply energy to the chromosphere and lower corona, where mode conversion processes can generate high-frequency transverse oscillations. Such energy redistribution mechanisms may play a significant role in chromospheric heating and could contribute to the long-standing problem of coronal heating.

Moreover, the results indicate pronounced damping of longitudinal p-modes near the photospheric layer, implying substantial leakage of acoustic energy into the overlying atmosphere. This supports the widely accepted scenario in which photospheric

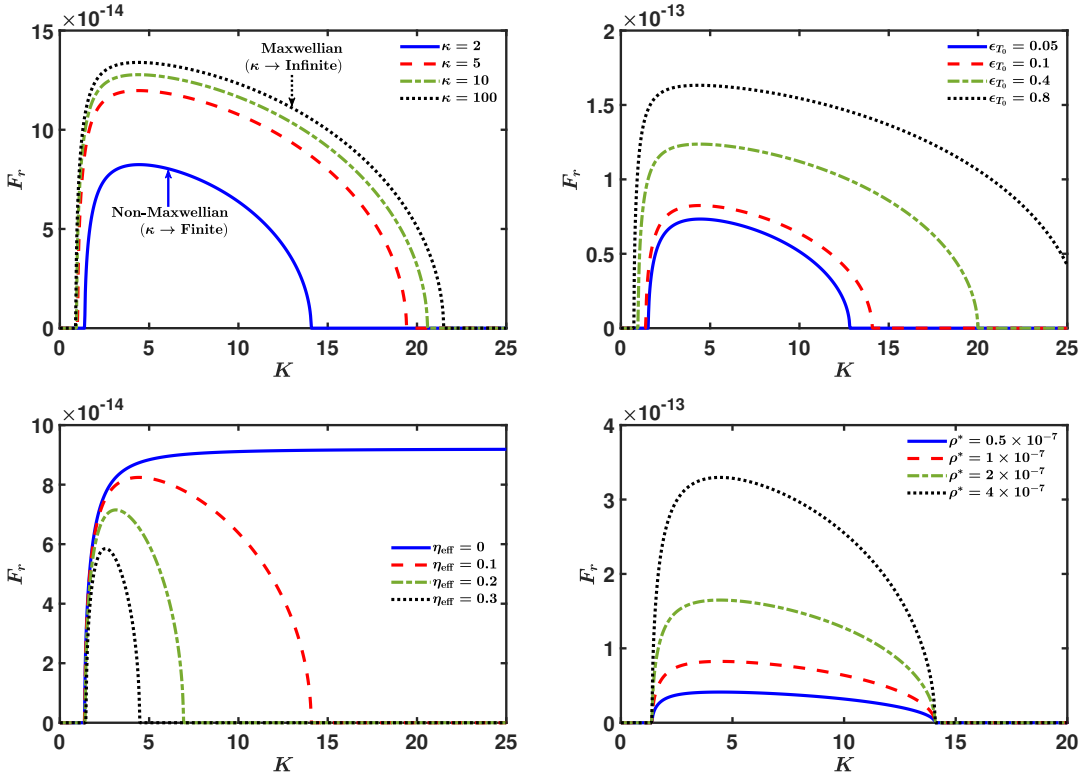


Figure 16. Profiles of the Jeans-normalized modal radiant energy flux density (F_r) as a function of the Jeans-normalized angular wavenumber (K) for different indicated values of the nonthermality spectral index (κ), solar equilibrium-to-electron temperature ratio (ϵ_{T_0}), effective dynamic viscosity (η_{eff}), and normalized surface fluid density (ρ^*) associated with the solar surface plasma fluctuations at $\xi = 2.25$.

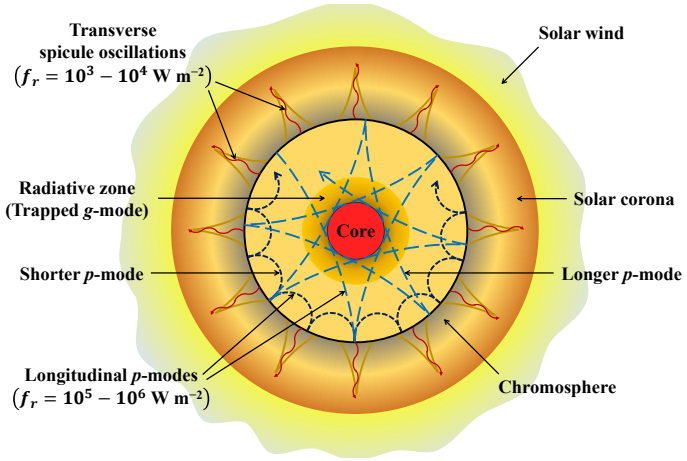


Figure 17. A schematic diagram of the Sun depicting g-modes, p-modes, and spicule oscillations in different solar constitutive concentric zones. The shorter p-mode and longer p-mode are indicated with square dotted and long dashed lines, respectively. The g-mode is trapped inside the radiative zone in the adjacent concentric spherical layer surrounding the solar core.

p-mode oscillations supply energy to the chromosphere and lower corona, where mode conversion processes can generate high-frequency transverse oscillations. Such energy redistribution mechanisms may play a significant role in chromospheric heating and could contribute to the long-standing problem of coronal heating.

Figure 17 presents a schematic representation of the Sun and its concentric zones, illustrating the propagation characteristics of helioseismic modes. Shorter p-modes (dotted curves) propagate efficiently near the surface, while longer ones (dashed curves) penetrate deeper into the interior. In contrast, low-frequency g-modes remain trapped beneath the radiative zone. The schematic also highlights the generation and upward propagation of high-energy transverse spicules from the photosphere to the chromosphere and lower corona.

Overall, the graphical analyses (Figures 2–15) demonstrate that the inclusion of κ-distributed suprathermal electrons significantly modifies the modal characteristics of helioseismic waves compared to classical thermal models. Additionally, the combined effects of plasma turbulence, viscosity, electron temperature, and thermal conductivity introduce rich and previously unexplored features in solar plasma fluctuation dynamics. The present study thus provides new theoretical insights into the behaviour of both g- and p-modes within a κ-modified framework, contributing to an improved understanding of solar interior–atmosphere coupling.

A concise summary of the spatial characteristics of the various wave modes is presented in Table 4, while a synoptic overview of the modal properties is provided in Table 5. The roles of different stabilizing and destabilizing agents governing the solar plasma dynamics are summarized in Table 6.

Table 4. Spatial wave characteristics in different solar plasma regions

Wave type	Nature	Interior ($\xi < 2.25$)	Surface ($\xi = 2.25$)
Long waves (Gravitational)	Propagation	Strongly propagating ($\Omega_r \approx 1$)	Non-propagating ($\Omega_r = 0$)
	Dispersion	Dispersive	Non-dispersive
	Stability	Metastable ($\Omega_i = 0$)	Rapidly growing ($0 < \Omega_i < 1$)
Short waves (Acoustic)	Propagation	Strongly propagating ($\Omega_r > 2$)	Strongly propagating ($\Omega_r > 1$)
	Dispersion	Weakly dispersive	Non-dispersive
	Stability	Metastable ($\Omega_i = 0$)	Metastable ($\Omega_i = 0$)

Furthermore, our theoretical speculations of nonthermal solar plasma fluctuations show reasonable agreement with various solar observations reported in the literature[5,7,11–19,40,53,61–71]. A glimpse of the manifold solar observational and theoretical

Table 5. Characteristic properties of helioseismic wave modes

Helioseismic mode	K-range (normalized)	λ-range (m)	Regime	Velocity ($\mathrm{m\,s^{-1}}$)	Period (min)	Frequency (Hz)
Gravitational-like (g)	$K < 1.4$	$\lambda > 10^8$	$0 < \xi < 0.8$	$< 10^6$	120–160	$\leq 10^{-4}$
Acoustic-like (p)	$K > 1.4$	$\lambda < 10^8$	$0 < \xi < 2.25$	$\sim 10^5$	< 50	$\geq 10^{-3}$

Table 6. Parametric effects on the solar plasma oscillations

Parameter	Effect
Nonthermality spectral index (κ)	Stabilizer (accelerating agent)
Electron temperature (T_e)	Destabilizer (decelerating agent)
Effective dynamic viscosity (η_{eff})	Stabilizer (decelerating agent)
Effective thermal conductivity (κ^*_{Th})	Stabilizer (mixed influence)

data bolstering our analyses are concisely presented in Table 7.

5 CONCLUSIONS

In this study, a comprehensive semi-analytical investigation of acoustic wave fluctuations attributing to helioseismic wave dynamics in a self-gravitating, κ-distributed nonthermal solar plasma is systematically carried out. It is based on a unified viscoturbulent and thermally conductive plasma framework without invoking any kind of quasi-classic approximation. By incorporating suprathermal electron effects through the κ-distribution law, along with the ion fluid viscosity and thermal conductivity, a generalized set of nonlinear hydrodynamic equations is formulated. The subsequent linear normal spherical mode analysis leads to a cubic dispersion relation of a unique mathematical shape. Its dispersion coefficients encapsulate the coupled influences of nonthermality, self-gravity, thermal processes, viscosity, and geometrical curvature on the solar plasma fluctuation dynamics.

It is noteworthy that the modal features of the solar gravitational-like (long-wavelength) and acoustic-like (short-wavelength) waves are studied illustratively. The manifold features of the helioseismic collective waves and oscillations are investigated. Applying the Routh–Hurwitz (R-H) stability criterion, the stability behaviours of the solar plasmas under consideration is assessed analytically, with results in excellent agreement with the numerical findings illustrated in the corresponding graphical analyses. The plasma system is found to exhibit overall stability across spatiotemporal scales, primarily due to energy dissipation mechanisms associated with ion viscosity and thermal conduction.

The analysis reveals that nonthermal effects play a pivotal role in modifying the propagation and stability characteristics of helioseismic modes. In particular, the κ-parameter acts as a key regulator of the system dynamics. An increase in κ, corresponding to a plasma state closer to thermal equilibrium, enhances wave propagation and promotes stability. Conversely, stronger electron nonthermality ($\kappa \to 1.5$) and elevated electron temperature act as destabilizing factors in solar plasma fluctuation dynamics while exerting a decelerating influence on wave propagation. In contrast, plasma shear viscosity and thermal conductivity provide dissipative effects that suppress fluctuations and thereby enhance the overall stability of the system.

The numerical results demonstrate that the long-wavelength gravity modes (g-modes) remain confined within the solar interior (approximately within 2.4×10^8 m) and exhibit strong instability in the deeper solar regions, while the short-wavelength pressure modes (p-modes) propagate efficiently toward the surface with relatively stable oscillatory behaviours. In contrast, near the heliocentre, the system exhibits a metastable state, characterized by purely oscillatory modes, whereas a significant perturbation growth is observed in the intermediate interior regions due to gravitational effects. The study further establishes that wave dispersion is highly sensitive to radial position, with strong dispersive characteristics near the core and quasi-nondispersive behaviour at shorter fluctuation wavelengths.

A key outcome of this work is the evaluation of the helioseismic modal energy flux, demonstrating that the p-modes are capable of transporting substantial energy from the solar interior towards the solar surface. The corresponding estimated flux values lie in the range $f_r \sim 10^5 - 10^6\,\mathrm{W\,m^{-2}}$. These values are found to be consistent with observational predictions associated

Table 7. Comparison of our predictions with observations

S. No.	Item	Observation	Our prediction
1	Foundation	SSM	Plasma fluid model
2	Phase velocity at surface ($\xi = 2.25$)	10^4–$5\times10^4\,\mathrm{m\,s^{-1}}$	Up to $2\times10^5\,\mathrm{m\,s^{-1}}$
3	Phase velocity in the interior ($\xi \leq 2.25$)	Increases toward centre	Peaks near heliocentre and decreases with ξ
4	Phase velocity vs T_e	Decreases	Same trend
5	Phase velocity vs η_{eff}	Decreases	Same trend
6	Wavelength dependence (interior)	Long λ propagate faster	Same trend
7	Propagation vs κ	Increases	Same trend
8	Propagation vs ϵ_{T_0}	Increases	Same trend
9	Propagation vs η_{eff}	Decreases	Strongly reduced
10	Surface propagation	Short λ dominate	Same trend
11	Core propagation	Long λ dominate	Same trend
12	Growth in deep interior	No amplification	Metastable
13	Growth vs κ	Decreases	Same trend
14	Growth vs T_e	Increases	Similar trend
15	Growth vs η_{eff}	Decreases	Damped
16	Modal growth	Short λ stabilize faster	Long λ exhibit stronger growth
17	p-mode dominance	Up to the lower corona	Consistent
18	g-mode confinement	Within the radiative zone, $0 < r < 3\times10^8\,\mathrm{m}$	$r < 2.4\times10^8\,\mathrm{m}$
19	p-mode frequency	3.2–3.5 mHz	$\gtrsim 1$ mHz
20	g-mode frequency	0.02–0.1 mHz	$\lesssim 0.1$ mHz
21	g-mode energy	Concentrated near heliocentre	Peaks near core
22	T–λ relation	$T \approx 5$–7 min with $3\times10^7\,\mathrm{m} \leq \lambda \leq 4\times10^7\,\mathrm{m}$	$T \approx 8$–10 min with $3\times10^7\,\mathrm{m} \leq \lambda \leq 4\times10^7\,\mathrm{m}$
23	ν–k relation	$\nu \approx 3$–6 mHz with $k \approx 10^{-7}\,\mathrm{m^{-1}}$	$\nu \approx 3.7$ mHz with $k \approx 10^{-7}\,\mathrm{m^{-1}}$
24	Spicule phase speed	10^5–$1.5\times10^5\,\mathrm{m\,s^{-1}}$	10^4–$10^6\,\mathrm{m\,s^{-1}}$
25	Spicule energy flux	10^3–$10^4\,\mathrm{W\,m^{-2}}$	$f_r \sim 10^5 - 10^6\,\mathrm{W\,m^{-2}}$
26	Applicability	Modal parameterization	Modal conceptualization

with the spicule dynamics[19,20,61]. The results strongly support the hypothesis that photospheric p-mode oscillations can provide sufficient energy to drive transverse spicule motions through mode-conversion processes within the chromospheric layers. The enhanced damping of longitudinal modes near the surface further indicates efficient leakage of acoustic energy into the upper solar atmosphere, potentially contributing to chromospheric heating and the coronal energy budget.

Overall, this study highlights the critical importance of incorporating nonthermal plasma effects, viscosity, and thermal conductivity in modelling solar plasma dynamics. The obtained results provide new insights into the complex interplay between helioseismic wave propagation, plasma instability, and energy transport processes, thereby advancing our understanding of solar interior–atmosphere coupling. The present framework offers a robust foundation for future investigations into nonlinear wave interactions, turbulence-driven energy cascades, and realistic modelling of solar and astrophysical plasmas under non-equilibrium conditions.

The main concluding remarks derived from our presented theoretic analyses could be summarily given as:

(i) The thermal pressure-driven acoustic waves exist in the high-frequency regime where the self-gravitational fluctuation levels are gradually reduced. In such situations, all the gravitational interactions get transformed into the purely non-dispersive acoustic-like fluctuations known as the p-modes. This theoretical investigation provides a precise numerical derivation of the five-minute oscillation time period of such p-modes in confirmative with the solar observations.

(ii) Internal buoyancy-driven long gravitational waves having lower frequencies are found to exist at the deeper interior layers of the sun where the self-gravitational effect is highly active. Near the vicinity of heliocentre, these waves acquire maximum phase velocity, and beyond this region, they lose energy with the distance. Accordingly, these g-modes get trapped inside the solar interior, more precisely, within $\xi < 0.8$ ($r < 2.4\times10^8$ m), analogous to the case of a spherical cavity resonator[3]). Hence, our theoretical analyses exactly resemble the trapping of the internal gravity modes or g-modes inside the radiative zone. Here, the oscillation time period of this g-mode is obtained as, $\tau_p = 120 - 160$ min.

(iii) It is interestingly seen from the parametric variations that all the relevant solar parameters studied in this work, such as the electron nonthermality power spectral index (κ), equilibrium-to-electron temperature ratio $\left(\epsilon_{T_0}\right)$, dynamic viscosity ($\eta$), and thermal conductivity ($\kappa_{\rm Th}$) of the constitutive ionic fluid are observed to act as stabilizing agents on the entire solar plasmas. Moreover, κ and ϵ_{T_0} play the role of accelerating agents; whereas, η and T_e act as the decelerating sources on the solar plasma fluctuation dynamics.

(iv) Since the obtained helioseismic wave modes are linearly stable in broad K-scale, one can introduce nonlinear spherical analysis to see the solar nonlinear wave structures. Moreover, the consideration of local linear analysis is not proper to study the characteristic features of an inhomogeneous solar plasma system. Therefore, the inclusion of equilibrium inhomogeneity effects in our model could be more realistic in the solar-plasma oscillation study.

(v) Incorporating other significant nonextensive nonthermal distributions—such as generalized (r,q) distribution[72], regularized κ-distribution[73], and Kaniadakis distribution[74,75]—our analysis could offer deeper insights into nonthermal solar plasma dynamics and associated fluctuations.

(vi) It is a well-known fact that the temperature of the solar atmosphere increases rapidly from the lower layer (chromosphere) to the outmost layer (corona), while the density decreases accordingly[1,8,76]. The origin of this temperature–density anti-correlation remains unresolved and requires further investigation. Our suprathermal model may offer valuable insights into this enigmatic temperature inversion mechanism in the solar coronal regime[76].

(vii) Recent studies suggest that coherent harmonic motion of dark matter may resonantly excite solar (stellar) oscillation modes[77,78]. Its gravitational influence could impact solar plasma stability, paving the way for future investigations using refined coupled multi-fluid models.

(viii) Solar magnetic activity induces temporal variations in helioseismic data by altering global mode features associated with acoustic waves and oscillations[79]. In this context, our proposed suprathermal model may strengthen the investigative roadmap of the 11-year solar cycle characteristics by studying p-mode travel times and their evolution features.

(ix) A similar nonthermal analysis can be extensively extended to investigate various possible solar plasma instabilities[80], such as the drag instability, two-stream instability, Rayleigh–Taylor instability, Kelvin–Helmholtz instability, etc.

(x) The solar corona, with temperatures reaching $\sim 10^6$ K remains significantly hotter than the solar surface—a long-standing puzzle in solar physics. One proposed mechanism involves energy transfer via coupling between flux tubes and acoustic p-modes. Our analysis supports the idea that p-modes contribute to high-frequency transverse spicule oscillations, consistent with recent findings[21]. These non-radial modes may also play roles in broader solar phenomena such as flares, coronal mass ejection (CME)[81], and coronal heating mechanism.

In conclusion, despite the limitations discussed, the present study offers valuable insights into key collective dynamical processes in the nonthermal inhomogeneous solar interior plasmas, particularly in the presence of internal heating mechanisms such as fluid viscosity and thermal conductivity. Overall, this work establishes a foundational framework for interpreting helioseismic wave behaviour under nonthermal and dissipative conditions, and it opens promising avenues for future theoretical and observational investigations into solar plasma dynamics.

References

1. Stix, M. *The Sun* (Springer, Berlin, Heidelberg, 2002).
2. Bogdan, T. & Judge, P. Observational aspects of sunspot oscillations. *Philos. Transactions Royal Soc. A: Math. Phys. Eng. Sci.* **364**, 313–331, DOI: 10.1098/rsta.2005.1701 (2006).
3. Priest, E. *Magnetohydrodynamics of the Sun* (Cambridge University Press, 2014).
4. Hale, S. J., Chaplin, W. J., Davies, G. R., Elsworth, Y. P. & Howe, R. The next generation birmingham solar oscillations network (bison) spectrophotometer: a new miniaturized instrument for helioseismology. *RAS Tech. Instruments* **1**, 58–64, DOI: 10.1093/rasti/rzac007 (2022).
5. Christensen-Dalsgaard, J. Helioseismology. *Rev. Mod. Phys.* **74**, 1073–1129, DOI: 10.1103/RevModPhys.74.1073 (2002).
6. Bedding, T. R. & Kjeldsen, H. Solar-like oscillations. *Publ. Astron. Soc. Aust.* **20**, 203–212, DOI: 10.1071/AS03025 (2003).
7. Hansen, C. J., Kawaler, S. D. & Trimble, V. *Stellar Interiors* (Springer, New York, NY, 2004).
8. Aschwanden, M. J. *Chapter 11 - The Sun*, 235–259 (Elsevier, Boston, 2014), 3rd edn.
9. Bhattacharya, J. & Hanasoge, S. M. A spectral solver for solar inertial waves. *The Astrophys. J. Suppl. Ser.* **264**, 21, DOI: 10.3847/1538-4365/aca09a (2023).
10. Kosovichev, A. G. Inversion methods in helioseismology and solar tomography. *J. Comput. Appl. Math.* **109**, 1–39, DOI: 10.1016/S0377-0427(99)00152-1 (1999).
11. Kosovichev, A. G. Subsurface characteristics of sunspots. *Adv. Space Res.* **38**, 876–885, DOI: 10.1016/j.asr.2005.04.091 (2006).
12. Ulrich, R. K. The five-minute oscillations on the solar surface. *The Astrophys. J.* **162**, 993, DOI: 10.1086/150731 (1970).
13. Leibacher, J. W., Noyes, R. W., Toomre, J. & Ulrich, R. K. Helioseismology. *Sci. Am.* **253**, 48–57, DOI: 10.1038/scientificamerican0985-48 (1985).
14. Goldreich, P., Murray, N. & Kumar, P. Excitation of solar p-modes. *The Astrophys. J.* **424**, 466, DOI: 10.1086/173904 (1994).
15. Harvey, J. W. *et al.* The global oscillation network group (gong) project. *Science* **272**, 1284–1286, DOI: 10.1126/science.272.5266.1284 (1996).
16. Demarque, P. & Guenther, D. B. Helioseismology: Probing the interior of a star. *Proc. Natl. Acad. Sci.* **96**, 5356–5359, DOI: 10.1073/pnas.96.10.5356 (1999).
17. Basu, S. Global seismology of the sun. *Living Rev. Sol. Phys.* **13**, 2, DOI: 10.1007/s41116-016-0003-4 (2016).
18. Thompson, M. J. Helioseismology and the sun's interior. *Astron. Geophys.* **45**, 4.21–4.25, DOI: 10.1046/j.1468-4004.2003.45421.x (2004).
19. Pontieu, B. D., Erdélyi, R. & James, S. P. Solar chromospheric spicules from the leakage of photospheric oscillations and flows. *Nature* **430**, 536–539, DOI: 10.1038/nature02749 (2004).
20. Pontieu, B. D. *et al.* Chromospheric alfvenic waves strong enough to power the solar wind. *Science* **318**, 1574–1577, DOI: 10.1126/science.1151747 (2007).
21. Kuniyoshi, H., Shoda, M., Morton, R. J. & Yokoyama, T. Can the solar p-modes contribute to the high-frequency transverse oscillations of spicules? *The Astrophys. J.* **960**, 118, DOI: 10.3847/1538-4357/ad1038 (2024).
22. Shoda, M. & Yokoyama, T. High-frequency spicule oscillations generated via mode conversion. *The Astrophys. J.* **854**, 9, DOI: 10.3847/1538-4357/aaa54f (2018).
23. Dey, S. *et al.* Polymeric jets throw light on the origin and nature of the forest of solar spicules. *Nat. Phys.* **18**, 595–600, DOI: 10.1038/s41567-022-01522-1 (2022).

24. Riedl, J. M., Doorsselaere, T. V. & Santamaria, I. C. Wave modes excited by photospheric p-modes and mode conversion in a multi-loop system. *Astron. & Astrophys.* **625**, A144, DOI: 10.1051/0004-6361/201935393 (2019).

25. Gizon, L. & Birch, A. C. Local helioseismology. *Living Rev. Sol. Phys.* **2**, 6, DOI: 10.12942/lrsp-2005-6 (2005).

26. Ambastha, A. *Physics of the Invisible Sun* (CRC Press, Boca Raton, 2020).

27. Christensen-Dalsgaard, J. Solar structure and evolution. *Living Rev. Sol. Phys.* **18**, 2, DOI: 10.1007/s41116-020-00028-3 (2021).

28. Pierrard, V. & Lazar, M. Kappa distributions: Theory and applications in space plasmas. *Sol. Phys.* **267**, 153–174, DOI: 10.1007/s11207-010-9640-2 (2010).

29. Livadiotis, G. & McComas, D. J. Understanding kappa distributions: A toolbox for space science and astrophysics. *Space Sci. Rev.* **175**, 183–214, DOI: 10.1007/s11214-013-9982-9 (2013).

30. Lazar, M., Poedts, S. & Fichtner, H. Destabilizing effects of the suprathermal populations in the solar wind. *Astron. & Astrophys.* **582**, A124, DOI: 10.1051/0004-6361/201526509 (2015).

31. Livadiotis, G., Desai, M. I. & Wilson, L. B. Generation of kappa distributions in solar wind at 1 au. *The Astrophys. J.* **853**, 142, DOI: 10.3847/1538-4357/aaa713 (2018).

32. Vasyliunas, V. M. A survey of low-energy electrons in the evening sector of the magnetosphere with OGO 1 and OGO 3. *J. Geophys. Res.* **73**, 2839–2884, DOI: 10.1029/JA073i009p02839 (1968).

33. Zouganelis, I., Maksimovic, M., Meyer-Vernet, N., Lamy, H. & Issautier, K. A transonic collisionless model of the solar wind. *The Astrophys. J.* **606**, 542–554, DOI: 10.1086/382866 (2004).

34. Tsallis, C. *Introduction to Nonextensive Statistical Mechanics* (Springer New York, New York, NY, 2009).

35. Livadiotis, G. & McComas, D. J. Beyond kappa distributions: Exploiting tsallis statistical mechanics in space plasmas. *J. Geophys. Res. Space Phys.* **114**, A11105, DOI: 10.1029/2009JA014352 (2009).

36. Livadiotis, G. Kappa and q indices: Dependence on the degrees of freedom. *Entropy* **17**, 2062–2081, DOI: 10.3390/e17042062 (2015).

37. Rubab, N. & Murtaza, G. Debye length in non-maxwellian plasmas. *Phys. Scripta* **74**, 145–148, DOI: 10.1088/0031-8949/74/2/001 (2006).

38. Aman-Ur-Rehman & Lee, J. K. Electron acoustic waves in a plasma with a q-nonextensive distribution of electrons. *Phys. Plasmas* **25**, 022107, DOI: 10.1063/1.5012044 (2018).

39. Noble, L. M. & Scarf, F. L. Conductive heating of the solar wind. i. *Astrophys. J.* **138**, 1169, DOI: 10.1086/147715 (1963).

40. Whang, Y. C., Liu, C. K. & Chang, C. C. A viscous model of the solar wind. *The Astrophys. J.* **145**, 255, DOI: 10.1086/148760 (1966).

41. Craig, I. J. D. & Litvinenko, Y. E. Inflow reconnection solutions in incompressible visco-resistive plasmas. *The Astrophys. J.* **747**, 16, DOI: 10.1088/0004-637X/747/1/16 (2012).

42. Chandra, S. Investigation of diffusivity and viscosity in solar plasma. *Indian J. Phys.* **87**, 601–606, DOI: 10.1007/s12648-012-0239-3 (2013).

43. Roberts, B. & Campbell, W. R. Magnetic field corrections to solar oscillation frequencies. *Nature* **323**, 603–605, DOI: 10.1038/323603a0 (1986).

44. Pintér, B. Solar magnetic atmospheric effects on global helioseismic oscillations. *J. Astrophys. Astron.* **36**, 15–32, DOI: 10.1007/s12036-015-9331-3 (2015).

45. Das, S., Atteya, A. & Karmakar, P. K. A theoretic analysis of magnetoactive ges-based turbulent solar plasma instability. *Mon. Notices Royal Astron. Soc.* **523**, 5635–5660, DOI: 10.1093/mnras/stad1664 (2023).

46. Das, S. & Karmakar, P. K. Analysis of solar surface oscillations and energy transport with bispectral electronic thermostatistics. *The Astrophys. J.* **997**, 232, DOI: 10.3847/1538-4357/ae25ec (2026).

47. Adams, F. C., Fatuzzo, M. & Watkins, R. General analytic results for nonlinear waves and solitons in molecular clouds. *The Astrophys. J.* **426**, 629, DOI: 10.1086/174100 (1994).

48. Horedt, G. *Polytropes*, vol. 306 (Kluwer Academic Publishers, Dordrecht, 2004).

49. Larson, R. B. Turbulence and star formation in molecular clouds. *Mon. Notices Royal Astron. Soc.* **194**, 809–826, DOI: 10.1093/mnras/194.4.809 (1981).

50. Lizano, S. & Shu, F. H. Molecular cloud cores and bimodal star formation. *The Astrophys. J.* **342**, 834, DOI: 10.1086/167640 (1989).

51. Das, S. & Karmakar, P. K. Stability and wave dynamics in polytropic Eddington-inspired Born-Infeld gravitating solar plasmas. *Phys. Rev. E* **113**, 015205, DOI: 10.1103/2djh-d4qh (2026).

52. Baluku, T. K. & Hellberg, M. A. Dust acoustic solitons in plasmas with kappa-distributed electrons and/or ions. *Phys. Plasmas* **15**, 123705, DOI: 10.1063/1.3042215 (2008).

53. Litvinenko, Y. E. & Chae, J. Analytical description of nonlinear acoustic waves in the solar chromosphere. *Astron. & Astrophys.* **599**, A15, DOI: 10.1051/0004-6361/201629568 (2017).

54. Dwivedi, C. B., Karmakar, P. K. & Tripathy, S. C. A gravito-electrostatic sheath model for surface origin of subsonic solar wind plasma. *The Astrophys. J.* **663**, 1340–1353, DOI: 10.1086/511409 (2007).

55. Das, S. & Karmakar, P. K. Non-planar magnetoactive ges-based solar plasma stability. *J. Astrophys. Astron.* **43**, 44, DOI: 10.1007/s12036-022-09838-3 (2022).

56. Braginskii, S. I. *Transport processes in a plasma*, vol. 1, 205–311 (Consultants Bureau, New York, 1965).

57. Hartle, R. E. & Sturrock, P. A. Two-fluid model of the solar wind. *The Astrophys. J.* **151**, 1155–1170, DOI: 10.1086/149513 (1968).

58. Clark, R. N. The Routh-Hurwitz stability criterion, revisited. *IEEE Control. Syst. Mag.* **12**, 119–120 (1992).

59. Guillemin, E. A. The mathematics of circuit analysis. *John Wiley, New York, Lond.* (1949).

60. Cook, M. V. Flight dynamics principles: a linear systems approach to aircraft stability and control. *Butterworth-Heinemann* (2012).

61. He, J.-S. *et al.* Upward propagating high-frequency Alfvén waves as identified from dynamic wave-like spicules observed by sot on *hinode*. *Astron. & Astrophys.* **497**, 525–535, DOI: 10.1051/0004-6361/200810777 (2009).

62. Zhugzhda, Y. D. & Stix, M. Acoustic waves in structured media and helioseismology. *Astron. Astrophys.* **291**, 310–319 (1994).

63. Hill, F. *et al.* The solar acoustic spectrum and eigenmode parameters. *Science* **272**, 1292–1295, DOI: 10.1126/science.272.5266.1292 (1996).

64. Chen, P. F. & Priest, E. R. Transition-region explosive events: Reconnection modulated by p-mode waves. *Sol. Phys.* **238**, 313–327, DOI: 10.1007/s11207-006-0215-1 (2006).

65. Kitiashvili, I. N., Kosovichev, A. G., Mansour, N. N. & Wray, A. A. Excitation of acoustic waves by vortices in the quiet sun. *The Astrophys. J. Lett.* **727**, L50, DOI: 10.1088/2041-8205/727/2/L50 (2011).

66. Viñas, A. F., Gaelzer, R., Moya, P. S., Mace, R. & Araneda, J. A. *Chapter 7 - Linear Kinetic Waves in Plasmas Described by Kappa Distributions*, 329–361 (Elsevier, 2017).

67. Duckenfield, T. J., Kolotkov, D. Y. & Nakariakov, V. M. The effect of the magnetic field on the damping of slow waves in the solar corona. *Astron. & Astrophys.* **646**, A155, DOI: 10.1051/0004-6361/202039791 (2021).

68. Griffiths, M., Gyenge, N., Zheng, R., Korsós, M. & Erdélyi, R. p-mode oscillations in highly gravitationally stratified magnetic solar atmospheres. *Physics* **5**, 461–482, DOI: 10.3390/physics5020032 (2023).

69. Mikhalyaev, B. B., Derteev, S. B., Shividov, N. K., Sapraliev, M. E. & Bembitov, D. B. Acoustic waves in a high-temperature plasma ii. damping and instability. *Sol. Phys.* **298**, 102, DOI: 10.1007/s11207-023-02196-5 (2023).

70. Zhao, L.-L., Zank, G. P., Nakanotani, M. & Adhikari, L. Observations of waves and structures by frequency–wavenumber spectrum in solar wind turbulence. *The Astrophys. J.* **944**, 98, DOI: 10.3847/1538-4357/acb33b (2023).

71. Zhao, L., Zank, G. & Li, H. Non-propagating structures and propagating waves in solar wind turbulence revealed by simulations and observations. *Rev. Mod. Plasma Phys.* **9**, 24, DOI: 10.1007/s41614-025-00200-y (2025).

72. Qureshi, M. N. S., Shah, H. A., Murtaza, G., Schwartz, S. J. & Mahmood, F. Parallel propagating electromagnetic modes with the generalized (r,q) distribution function. *Phys. Plasmas* **11**, 3819–3829, DOI: 10.1063/1.1688329 (2004).

73. Scherer, K., Fichtner, H. & Lazar, M. Regularized κ-distributions with non-diverging moments. *Europhys. Lett.* **120**, 50002 (2018).

74. Dubinov, A. E. Gas-dynamic approach to the theory of non-linear ion-acoustic waves in plasma with Kaniadakis' distributed species. *Adv. Space Res.* **71**, 1108–1115 (2023).

75. Irshad, M. *et al.* Effect of κ-deformed Kaniadakis distribution on the modulational instability of electron-acoustic waves in a non-Maxwellian plasma. *Phys. Fluids* **35** (2023).

76. Barbieri, L., Casetti, L., Verdini, A. & Landi, S. Temperature inversion in a gravitationally bound plasma: Case of the solar corona. *Astron. & Astrophys.* **681**, L5 (2024).

77. Kalashnikov, I. Y. & Chechetkin, V. M. Influence of dark matter on gravitational stability of isothermal gas clouds. *Mon. Notices Royal Astron. Soc.* **514**, 1351–1358 (2022).

78. Sakstein, J. & Saltas, I. D. Dark matter induced stellar oscillations. *Mon. Notices Royal Astron. Soc. Lett.* **527**, L14–L18 (2023).

79. Vasilyev, V. & Gizon, L. Detecting stellar activity cycles in p -mode travel times. *Astron. & Astrophys.* **682**, A142, DOI: 10.1051/0004-6361/202346854 (2024).

80. Ru, C. Q. On kelvin-helmholtz instability of particulate two-fluid flow. *Acta Mech. Sinica* **41**, 324143 (2025).

81. Ahamed, A. A. *et al.* Study of solar activities associated with a Halo CME on 17 Feb 2023 event. *New Astron.* **114**, 102312 (2025).

82. Cairns, R. A. The role of negative energy waves in some instabilities of parallel flows. *J. Fluid Mech.* **92**, 1–14, DOI: 10.1017/S0022112079000495 (1979).

Funding statement

This work has not been supported by any funding agency.

Acknowledgements

The authors appreciatively acknowledge the cooperation received from Tezpur University. The dynamic help and support from the colleagues in the Astrophysical Plasma and Nonlinear Dynamics Research Laboratory (APNDRL), Department of Physics, Tezpur University, is duly recognized. S.D. wholeheartedly acknowledges the Department of Science and Technology (DST), Government of India, for the DST-INSPIRE research fellowship (Grant: DST/INSPIRE Fellowship/2021/IF210234). The award of IUCAA Associateship, Pune, India, to P.K.K, is gratefully appreciated.

Author contributions statement

S.D. conceptualized the study, designed the methodology, performed the numerical analysis, and drafted the main manuscript text. P.K.K. contributed to the theoretical framework, interpreted the results, and supervised the research. A.A. contributed to the discussions, analytical development, and critical revision. All authors reviewed and approved the final version of the manuscript.

Data availability

All data generated or analysed during this study are included in this published article.

Competing interests

The authors declare no competing interests.

A Ultra-low frequency (ULF) analysis

At ultra-low frequency ($\Omega << 0$) regime, the Jeans-normalized real and imaginary angular frequency parts of the collective acoustic wave fluctuations propagating on the self-gravitationally bounded solar spatiotemporal scale can be expressed as

$$\Omega_r \approx 0, \tag{28}$$

$$\Omega_i \approx \frac{(1-\gamma)\left[1-\left(2\epsilon_{T_0}+\alpha^{-1}\right)\left(K^2+\xi^{-2}\right)\right]\kappa^*_{\rm Th}K^2}{1-(\gamma-1)\eta_{\rm eff}\kappa^*_{\rm Th}K^2\left(K^2+2/\xi^2\right)-\left(\gamma\epsilon_{T_0}+\alpha^{-1}\right)\left(K^2+\xi^{-2}\right)}. \tag{29}$$

B Larson logabarotropic equation of state

Spectroscopic observations suggest that the spectral linewidth in diffused molecular clouds scales with material density following an empirical power-law relation, as reported in previous studies[47,49,50], expressed in standard notation as

$$\Delta v \propto \rho^{-1/2}. \tag{30}$$

This correlation can be interpreted as the effective fluid transport speed in the considered turbulent astrofluid medium cast as

$$\Delta v = v_{\rm turb} = \left(\frac{dp_{\rm turb}}{d\rho}\right)^{1/2} \propto \rho^{-1/2}, \tag{31}$$

$$\text{or, } \frac{dp_{\rm turb}}{d\rho} \propto \rho^{-1}, \tag{32}$$

$$\text{or, } \frac{dp_{\rm turb}}{d\rho} = p_0\rho^{-1}, \tag{33}$$

where, p_0 is a proportionality constant designating the equilibrium fluid pressure. Integrating Equation (33), the Larson logabarotropic equation of state for a turbulent astrofluid can be obtained with all the customary notations as

$$p_{\rm turb} = p_0 \ln\left(\frac{\rho}{\rho_0}\right). \tag{34}$$

Herem ρ_0 denotes the mean (equilibrium) volumetric density of the fluid matter obtained at $p_{\rm turb} = 0$. It may herewith be immediately conjectured that $p_{\rm turb} = 0$, if $\rho = \rho_0$. Thus, it is evident that the fluid equilibrium here is far away from being in a turbulent (intermittent) state.

C Negative energy mode analysis

Cairns has demonstrated a criterion to identify the presence of negative energy wave modes in waveguide systems[82]. According to this criterion, a specific mode is classified as a negative energy wave if it satisfies the condition:

$$C = \Omega\frac{\partial D}{\partial \Omega} < 0. \tag{35}$$

Here, C denotes the characteristic function of the corresponding mode, while $D(\Omega, K)$ represents the dispersion function for a given wavenumber K. The dispersion relation of the system is defined by the condition $D(\Omega, K) = 0$.

The dispersion function for the collective helioseismic modes propagating through the solar plasmas can be expressed using standard notations as

$$D(\Omega, K) = A_3\Omega^3 + A_2\Omega^2 + A_1\Omega + A_0. \tag{36}$$

Hence, the first order differentiation of $D(\Omega, K)$ with respect to Ω is obtained as

$$\frac{\partial D}{\partial \Omega} = 3A_3\Omega^2 + 2A_2\Omega + A_1. \tag{37}$$

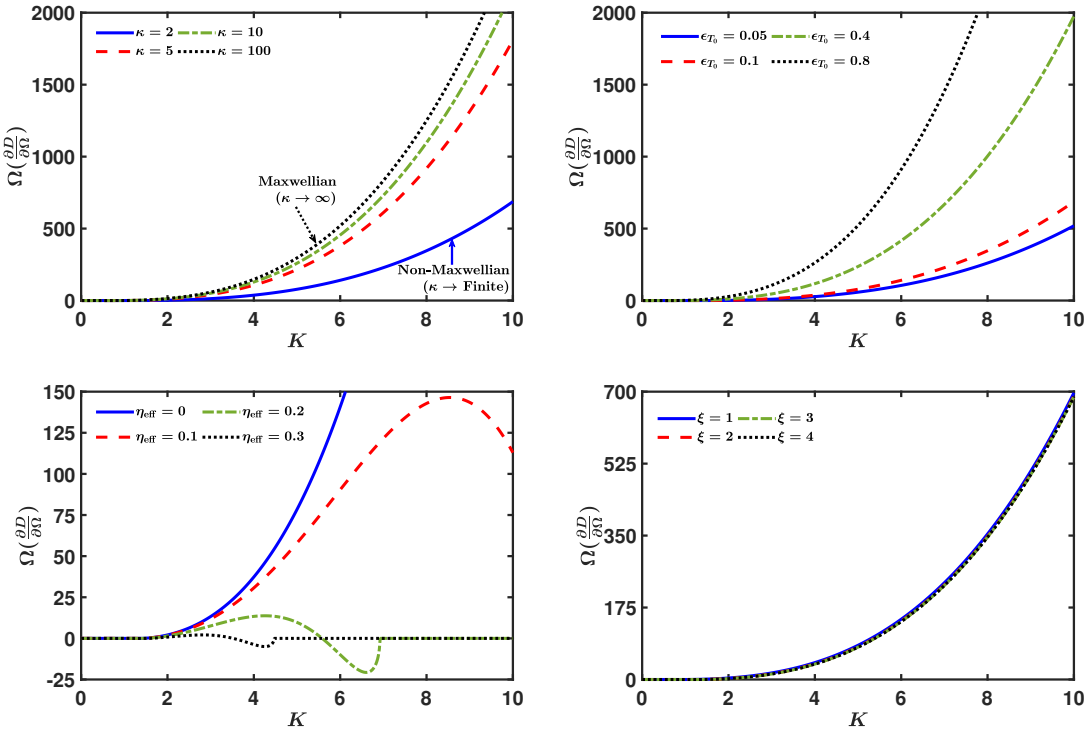


Figure 18. Profiles of the dispersion characteristic function $C = \Omega(\partial D/\partial\Omega)$ of the solar plasma fluctuations with variation in the Jeans-normalized angular wavenumber (K) for different judicious indicated values of nonthermality spectral index (κ), temperature ratio $\left(\epsilon_{T_0}\right)$, effective dynamic viscosity (η_{eff}), and Jeans-normalized radial distance (ξ).

Hence, for negative energy wave modes to exist in the solar interior plasma, Equation (35) must be satisfied within this regime. The parametric variations of the characteristic function C with K are depicted in Figure 18. As shown in Figure 18, for different indicated values of κ, ϵ_{T_0}, and ξ, the parameter C remains entirely positive across the bounded solar plasma spatiotemporal scale, indicating the absence of negative energy wave modes. However, for higher values of η_{eff}, negative energy modes do appear, consistent with the constraints of the energy conservation law. As the dynamic viscosity increases, the fluid experiences greater resistance. It reduces the positive wave energy of collective oscillations, leading to a gradual decrease in wave amplitude over time. Consequently, negative energy modes emerge, contributing to the overall stability of the system.